MOPITT

Measurement of Pollution in the Troposphere

Algorithm Theoretical Basis Document

Retrieval of Carbon Monoxide Profiles and Column Amounts from MOPITT Observed Radiances

(Level 1 to Level 2)

G. L. Francis, M. N. Deeter, S. Martínez-Alonso, J. C. Gille,

D. P. Edwards, D. Mao, H. M. Worden, and D. Ziskin

Atmospheric Chemistry Observations and Modeling Laboratory

National Center for Atmospheric Research

Boulder, Colorado

June 2017

Contents

List of Figures

List of Tables

1 Introduction

The purpose of this document is to describe and provide the theoretical basis for the algorithms that are used to produce the MOPITT Level 2 (L2) retrieved carbon monoxide (CO) products from the calibrated Level 1 (L1) measured radiances. This updates the previous L1-L2 ATBD, dated 1996, which was written well before the MOPITT launch on Terra in December 1999. That document had the purpose of providing the basis for the original algorithms. It therefore did not incorporate the results of instrument parameters determined later, nor lessons learned from experience of the instrument in orbit.

An overview of the MOPITT experiment objectives is first presented in Section 2.1, followed by some historical background in Section 2.2. Section 2.3 contains a summary description of the MOPITT instrument. Correlation spectroscopy relevant to MOPITT is summarized in Section 2.4. The MOPITT L1-L2 data algorithms are then discussed in Section 3. Section 3.1 describes the radiative transfer modeling and the MOPITT forward model for both the CO thermal channels and the CO and CH_4 solar channels. In Section 3.2 the cloud detection and clearing algorithm is presented, describing how MOPITT determines clear and cloud-contaminated scenes. Section 3.3 presents the retrieval algorithms and their evaluation for the CO channels. No CH_4 data product is currently produced, as discussed below.

2 Overview and Background Information

2.1 Experiment Objectives

2.1.1 Quantitative Objectives

The objectives of the MOPITT experiment are: 1) Retrieving vertical profiles of CO with a horizontal resolution of ~22x22 km^2, a 3 km vertical resolution, and an accuracy of 10% throughout the troposphere. The CO tropospheric columns are obtained using thermal-infrared (TIR) MOPITT channels near 4.7 μm, and are therefore available both day and night; 2) Retrieving CO tropospheric total column measurement with the same horizontal resolution and 10% accuracy; 3) Retrieving CH_4 total column with the same horizontal spatial resolution and a precision better than 1%. The CO and CH_4 column retrievals require measurements in the near-infrared (NIR) MOPITT channels near 2.2 μm and 2.3 μm respectively, and are therefore only available on the sunlit side of each orbit.

2.1.2 Importance of CO

CO is photochemically active and plays an important role in tropospheric chemistry. It is a component of HO_x chemistry, affecting concentrations of the OH radical and OH/HO_2 partitioning. The OH radical is a key tropospheric agent involved in the removal of various forms of natural and anthropogenic pollution. CO is also a component in tropospheric O_3 formation through oxidation of CO and CH_4. With a natural lifetime from weeks to months, depending on season and latitude, globally evolving CO concentrations are a useful tracer for diagnosing long-range chemical transport and deep convection. The lifetime provides a useful timescale to quantify seasonal CO sources and sinks globally. The relationship between CO and CH_4 provides a possibility for studying the role played by CH_4 in climate forcing.

MOPITT measurements provide a unique resource to enhance our knowledge of tropospheric chemistry and how it interacts with surface/ocean/biomass systems, atmospheric transport, and the carbon cycle. Global CO measurements from MOPITT can also be applied to operational data assimilation systems, or to an OSSE (Observation System Simulation Experiment) [Edwards et al., 2009] to assess space-borne measurement concepts for future missions.

2.1.3 Importance of CH_4

Atmospheric methane is both chemically and radiatively important. It has a long lifetime in the troposphere and is well mixed. In addition, most CH_4 sources are relatively small. As a result it is necessary to measure methane with a precision better than 1% so that variations showing sources and sinks can be detected.

Early work to retrieve MOPITT CH_4 showed that detection was possible but could not satisfy the 1% requirement. This is due to at least three effects: geophysical noise [Deeter et al., 2009], the spectral variation of the reflectivity across the filter passband [Pfister et al., 2005] , and polarization (especially over the ocean). These difficulties have not yet been overcome, so no CH_4 product is being produced at this time. Discussion of CH_4 is included to allow for future applications.

2.2 Historical Perspective

It has long been known that it is possible to estimate the amount of a trace gas in the atmosphere by measuring its infrared absorption spectrum. The problem is often that the spectral lines of the gas of interest are obscured by the lines and bands of other gases. Detection by gas absorption using a thermopile detector was suggested early by Pfund [1939]. Independently, Luft [1943] showed that a gas absorption cell could be used with an ingenious acoustic capacitor to measure CO, CO_2 and several hydrocarbons. Smith and Pidgeon [1964] proposed chopping the incoming beam with a cell containing the target gas to enhance the sensitivity of the instrument to the target gas. This was subsequently implemented in the Oxford Selective Chopper Radiometer (SCR) that flew on Nimbus 4 [Abel et al., 1970] as well as Nimbus 5 and several generations of NOAA TIROS satellites. These can be thought of as precursors to the MOPITT Length-Modulated Radiometers (LMRs).

Simultaneously, in the early 1960's Goody developed a different approach, in which a beam of solar radiation passed through a cell containing N_2O. By modulating the pressure, only the absorption of the signal at the N_2O lines was affected, permitting an estimate of the atmospheric N_2O column and its seasonal variation. The method and results were not published until later [Goody, 1968, 1969] This idea was also used by Oxford in their Pressure Modulated Radiometer (PMR) that flew on Nimbus 6, Nimbus 7, and ISAMS, and was a direct precursor to the MOPITT PMRs. The 1971 NASA Working Group on the Remote Measurement of Pollution [Katzoff, 1971] describes an independent development of this technique in the same time period.

The possibility of remotely measuring tropospheric CO profiles from space using thermal infrared radiation was first suggested by Ludwig et al. [1974]. This was followed by a 1979 airborne instrument for measuring CO [Reichle et al., 1986a], and the Measurement of Air Pollution from Satellites (MAPS) onboard the second Space Transport System engineering test flight (STS-2) of the NASA Space Shuttle in November 1981. MAPS was a gas filter radiometer operating in the 4.7 μm region of the CO fundamental band (0-1) with a passband from 2080 to 2220 cm^{-1}. At the surface the instantaneous field of view was approximately ~20x20 km^2. It successfully demonstrated the feasibility of inferring the CO profile using nadir-viewing geometry. Subsequent MAPS experiments provided additional global tropospheric CO measurements and further demonstrated the importance and feasibility of CO measurements from space.

The MAPS experiments provided important early CO measurements for global tropospheric chemistry study. Their success made clear that improvements were important and justifiable: MAPS had limited spatial coverage and retrieved only the average CO mixing ratio in the middle of the troposphere. A multiple-level CO profile retrieval, obtained from low-earth-orbit that would resolve the troposphere into several layers was needed. MOPITT was designed to meet this requirement.

2.3 The MOPITT Instrument

The MOPITT instrument makes use of the "selective chopping principle". Drummond [1992] gives a conceptual description of the instrument, discussing the PMR used to sound the upper levels of the

troposphere where the pressure is low, and the LMR that provides information on levels closer to the surface with higher pressures. More detailed descriptions of the LMR, which was developed initially for MOPITT, are contained in Drummond [1989] and Tolton and Drummond [1997].

In the next section we describe the instrument's state at launch. This is followed by a summary of changes in the instrument over the length of the mission, as is frequently the case, due to time in the harsh space environment. We also indicate how these instrument changes are handled through modifications of the MOPITT processing algorithms.

2.3.1 MOPITT at Launch

A block diagram of MOPITT as launched is shown in Figure 2. It consists of two optical tables that are mirror images. Two scan mirrors on each table direct signals into optical trains, each with dichroic beam splitters, two LMCs and a PMC, creating four channels and eight signals per table. Each signal in turn is passed to four detectors that each subtend a ∼22x22 km^2 pixel at the surface at nadir. The detectors lie in a one-dimensional array along the direction of motion; the mirrors move in unison to scan these detector arrays in the cross-track direction, giving the scan pattern shown in Figure 3.

To obtain the required sensitivity, the detectors and their band-defining filters are cooled to ∼85K by a Stirling cycle cooler on each bench. These are arranged so their mechanical motions balance each other. The sixteen detectors and filters on each bench are clustered on the cold head of that cooler.

In addition to performing cross-track scans of the earth, the scan mirrors turn to space every ten scans, providing a cold calibration point to give the radiometric offset, and turn to an internal black body at the instrument temperature after every fifth space view to get a warm calibration point, and thus a determination of the radiometer gain for the thermal channels. The internal target is not hot enough to provide a calibration signal for the 2 μm channels; for these the target is heated to 460 K, a so-called "hot calibration", but this is only needed infrequently, depending on the rapidity of the build-up of ice on the cold filters. Nominal channel characteristics are summarized in Table 1.

MOPITT was launched on the Terra satellite on 18 December 1999. Terra achieved its nominal 705 km altitude at the end of 2000 February. The doors were then opened for further outgassing. MOPITT was placed in Science mode on 2 March 2000.

During its first fourteen months in orbit MOPITT carried out several calibration events [Drummond et al., 2010]. Each began with a hot calibration, followed by a decontamination, during which the coolers are turned off and the cold heads are allowed to warm to ambient temperatures. This allows any ice that has formed (which reduces the channel throughput) to sublimate. A second calibration after the decontamination is carried out to confirm that the throughput has been restored [Drummond et al., 2010, 2016].

2.3.2 MOPITT Phase 2

One of the coolers failed on 7 May 2001; this resulted in loss of the four channels on Table 1. The instrument was then placed in Standby mode and tests carried out, but no data were taken until August.

Chopper 3 failed on 4 August, fortuitously in the open position, during engineering tests prior to restarting MOPITT with one cooler (the other arranged so its piston moved passively to balance vibration). Because the signals are digitized at an early stage, and because the InSb detectors have low 1/f noise, it proved possible to use the LMC modulation to get the desired variable signal. This did not require any modification to the algorithms.

After the instrument was restarted on 24 August, only Channels 5-8 provide useful data. This is referred to as "Phase 2". At this time the pressure in the Channel 7 PMC was increased to improve sounding in the upper troposphere [Drummond et al., 2010].

Three other significant anomalies have ocurred since launch. First, on 28 July 2009 another cooler anomaly occurred when the displacer of the inoperative cooler hit the end of the cylinder, causing it to stop. This was solved by slightly reducing the drive of the operating cooler. This resulted in more

vibration being imparted to Terra, but no adverse effects have been reported. Second, the LMC3 sieve heater failed on 3 October 2009, but no change in the instrument was required. Third, during the hot calibration sequence the resonant frequency of the PMC is measured in order to determine its mean gas pressure. This indicates a slow decrease in pressure, which can be partially explained by the decrease in temperature, but also indicates there is probably a slow gas leak. The pressures in the LMCs can be measured directly, and have dropped as well. Initially this is associated with a temperature decrease, but in recent years again may indicate a slow leak of gas from the cell. These are corrected by making time-dependent changes to the forward model algorithms, as described in Section 3.1.11

2.4 Correlation Spectroscopy

MOPITT measures upwelling thermal emission from the atmosphere and surface in the longwave channels, and reflected solar radiation in the shortwave channels. The latter has passed through the atmosphere, been reflected at the surface, and transmitted back up through the atmosphere. Total atmospheric transmittance derived from reflected sunlight measurements is an effective way to determine the total column amount of a trace gas. This technique requires that the target gas has a spectral band in a region with large solar radiance, and that the total optical depth along such a path is not too large. CH_4 has an overtone band near 2.2 μm with a measurable, but not excessive, total absorption for such a path. Similarly, CO has its first overtone band at 2.3 μm which is also suitable. For vertical profiling the requirement is that significant and measurable portions of the signal must originate in different atmospheric layers, which means there must be several values of different but appreciable opacity in the atmosphere, and that there must also be a source of radiation in the atmosphere. Thermal emission is a radiation source, and the CO fundamental band at 4.7 μm has enough opacity to determine atmospheric amounts [Reichle et al., 1986b, 1990].

All three MOPITT CO and CH_4 bands lie in regions of the spectrum containing other bands, and the lines of the gases of interest are mixed with those of interfering species. It would be possible, in principle, to measure the total emission or transmission of the species of interest, and correct for the contributions of the interfering species. However, the contributions of other species are often larger than those of the gases of interest, and their amounts are often not known with sufficient accuracy. The uncertainties of the corrections may significantly degrade, or even mask, changes due to the gas of interest.

MOPITT is designed to meet this challenge by enhancing the sensitivity of the instrument to the gas of interest. Since all gases in the atmosphere are emitting and absorbing simultaneously, it is essential that the effect of the gas of interest be separated out from the general radiation field. Further, since information about the vertical distribution of the gas is contained in the shape of an individual absorption/emission line, it is necessary to be able to resolve the line shape, which generally requires high spectral resolution. High spectral resolution leads to low signal-to-noise, which means low instrument sensitivity. Therefore, high sensitivity and high spectral resolution requirements for tropospheric trace species remote sensing are difficult to implement with conventional dispersing instruments.

Correlation Spectroscopy offers the opportunity for high spectral resolution as well as high signal-to-noise [Edwards et al., 1999]. In this approach, a cell contains a target gas through which passes a radiation stream. By cycling the amount of gas in the cell between two states, the detector will alternately look through two different filters. The difference of the two signals will be identical to the output of a system in which the gas cell and its modulator are replaced by an equivalent optical filter (a "Difference Transmittance" [D]) with the following unique characteristics:

(1) The "equivalent filter profile" is zero between the spectral lines of the gas in the cell, eliminating signals from spectral regions subject to interference by other species.

(2) The filter profile has a maximum at each spectral line; therefore the energy from each spectral line in a broadband emission is collected simultaneously. As a result, the system is very sensitive to

radiation with a spectrum identical or similar to that of the gas in the cell. Obviously the spectrum of the gas itself is best correlated with the filter profile.

(3) The apparatus does not require any high precision optical adjustments. All that affects the alignment is Doppler shift caused by relative motion between gas in the cell and the emitting atmospheric gas.

(4). The shape of the equivalent filter is sensitive to the amount of gas in the cell. If small amounts of gas are placed in the cell, the spectral lines will be narrow with incomplete absorption at the centers of the lines. The D-transmittance will have peaks in line centers, where absorption coefficients are largest. If larger amounts of gas are placed in the cell, the lines will be broader and completely absorbed in the centers. In this case, the D-transmittance will have peaks in the line wings, where absorption coefficients are smaller. By placing different amount of gas in the cell, different parts of the spectral line will be sampled, leading to altitude discrimination and vertical resolution. The largest part of the upwelling signal emitted by the atmosphere comes from the altitude region in which the optical depth is near unity. Therefore, a cell that is sensitive to the line center will respond to signals originating higher in the atmosphere, while a cell with larger amounts of gas will respond to signals originating in the wings of the pressure broadened lines, at higher pressures (lower altitudes).

The average of the signals obtained at the two states of the correlation cell can also be obtained. The resulting "Average Transmittance" (A) has the property that its transmittance is nearly unity away from the lines in the cell, but it reduces the signals at the centers of the lines. Thus, it is sensitive to other gases, and especially to the surface contribution to the upwelling radiation in the spectral regions of interest.

MOPITT makes use of two methods to modulate the gas transmittance. The first involves altering the pressure using "pressure modulated cells" [Taylor, 1983]. The second involves altering the length of the gas optical path using "length modulated cells" [Drummond, 1989]. MOPITT uses two PMRs with different mean pressures, and four LMRs. Dichroic filters separating the 2 μm and 4.7 μm channels yield eight separate spectral channels. The channel characteristics are summarized in Table 1. Each channel produces an A and a D signal.

Pressure Modulator Cell technology has flown on numerous satellite missions extending back to Nimbus 4 (1970), Nimbus 5 (1972), Nimbus 6 (1975), Pioneer Venus (1978), and the Upper Atmosphere Research Satellite (UARS) in 1991. Extensive laboratory experimental studies to understand the operation of the cells have been conducted by many groups. Models and calibration techniques of different complexity have been developed. The mean and modulated transmission function of a pressure modulator cell were first measured during operation in 1988 using a tunable diode laser spectrometer [May et al., 1988]. Good agreement was obtained between theoretical calculations and measurements. A detailed investigation of the variation of pressure, temperature, and transmission within a pressure modulator was released in 1989 [Roscoe and Wells, 1989]. Berman et al. [1993] made precise spectral line measurements of CO in an operating PMC using spectroscopic techniques. They also showed that gas amounts and pressure in a PMC can be accurately measured after filling and sealing. This demonstrates a method for noninvasive monitoring of gas purity and amount during ground testing of satellite instrumentation. These studies clearly show that the operation of the PMC and the cell transfer function can be measured and modeled accurately.

During normal operation of an LMC there is no change of pressure in the sealed correlation cell. Instead, modulation is achieved by altering the optical path length. Temperature changes and slow leaks may occur in the LMC over time, but the pressure is monitored, and changes can be corrected in subsequent data processing, as described in Section 3.1.11.

(5). Although each detector measures the radiance through the target gas cell with both high and low amounts of gas, the signals are separated by filters into the rapidly varying difference (D) signal and the more slowly varying average (A) signal. Thus, each detector can be thought of as producing two signals. However, measurements through the high and low cells are made sequentially, not simultaneously: because MOPITT is moving more than 7 km/sec, the two measurements view scenes separated by $\sim$175 meters. This is of no importance for the atmosphere, but the underlying

surface temperature and emissivity can vary on these scales, resulting in "geophysical noise". As a first approach to reducing this effect, radiances measured during two sequential high (low) gas states are averaged to use with the radiances measured during the intermediate low (high) state to calculate the A and D values for that scene.

3 MOPITT Level 1 to Level 2 Data Reduction Algorithm Description

The entire chain of MOPITT data processing is depicted in Figure 1. Level 1 processing refers to the treatment of raw Level 0 data leading to calibrated Level 1 radiances, and is described in detail in the MOPITT Level 1 ATBD. Level 2 processing, described in detail in this section, refers to the techniques and algorithms by which Level 1 radiances ultimately yield a retrieval; that is, an estimate of the CO vertical profile expressed both as a set of volume mixing ratios on a defined grid and a total column value. The radiative transfer model relating MOPITT measured radiances to a variety of instrumental and atmospheric parameters is the foundation of the MOPITT retrieval algorithm and is described first in Section 3.1. Methods for identifying cloud-contaminated radiances, which are rejected in Level 2 processing, are then described in Section 3.2. Finally, details of the MOPITT optimal estimation-based retrieval algorithm are presented in Section 3.3.

3.1 Radiative Transfer Modeling

3.1.1 Physics of the Problem: Forward Model for Clear Sky Radiances

Atmospheric CO concentrations are typically 50-200 ppbv with substantially larger values possible in fire plumes or boundary layer inversions. With a characteristic lifetime of several weeks, the CO concentration can vary significantly over small spatial and temporal scales due to dynamical mixing and transport. In the case of CH_4, a substantial change in the concentration near the surface may result in only a small change in the total column above the source region. The measurement system must therefore maximize the total signal from these gases while using high spectral resolution to ensure sufficient sensitivity to changes in their concentration. This is best achieved using the gas correlation spectroscopy techniques described in Section 2.4.

As described briefly in Section 2.1.1, MOPITT makes measurements in three spectral regions. In more detail (and referring to the discussion in Section 2.4), a longwave thermal channel at 4.7 μm gives information about the tropospheric CO profile, while shortwave solar reflectance channels at 2.3 μm and 2.2 μm are designed to give information about CO and CH_4 total columns, respectively. Information in the CO channels can be combined to potentially improve the profile retrieval, because the shortwave sensitivity to near-surface CO complements the profile information in the longwave band.

The forward model provides a numerical simulation of the radiative transfer of the problem and a physical description of the measurement process. The purpose of the forward model is twofold. First, it is a critical tool for simulating and evaluating the measurement characteristics of the instrument; developing a forward model is an important step in the instrument design. Second, the forward model plays a central role in the operational data retrieval system. Inferring CO or CH_4 from the instrument signals is an inverse problem. An accurate forward model is essential for a successful retrieval.

3.1.2 The Radiative Transfer Equation

For the MOPITT spectral bands, the monochromatic radiance $I(\nu, h)$ at the top of the atmosphere (TOA) is described by the following radiative transfer equation:

$$I(\nu, h) = I(\nu, h_s)\tau(\nu, h_s) + \int_{h_s}^{h} B(\nu, T(z)) \frac{d\tau(\nu, z)}{dz} dz \tag{1}$$

Here $I(\nu, h_s)$ $[W/(m^2.sr.cm^{-1})]$ is the monochromatic radiance at the surface height h_s for wavenumber ν, the quantity h is the vertical distance between the instrument platform and the surface, $\tau(\nu, z)$ is the monochromatic atmospheric transmittance from z to h, and $B(\nu, T(z))$ is the Planck function $[W/(m^2.sr.cm^{-1})]$ at temperature $T(z)$. The first term on the right side of Equation [1] describes radiation reaching the instrument from the Earth's surface. The second term gives the contribution from atmospheric emission and absorption between the surface and the instrument. In this discussion all radiances are understood to be clear-sky values. The MOPITT approach for discriminating clear sky from clouds, and the algorithm for deriving clear sky radiances and cloud fractions under partially cloudy conditions, is described in Section 3.2.

The boundary radiance term in Equation [1] has two components:

$$I(\nu, h_s) = \epsilon B(\nu, T_s) + (1 - \epsilon) I_b(\nu, h_s) \tag{2}$$

Here ϵ is the surface emissivity (assumed constant in each MOPITT passband), T_s is the surface temperature, and I_b is the downward radiance reaching the surface. I_b is the sum of a solar contribution together with the downwelling thermal emission from the atmosphere. The relative importance of the two terms in Equation 2 varies strongly with wavenumber. This is illustrated in Figure 1 of Pan et al. [1995]. At longer wavelengths, where the solar spectrum is weak and the ground reflectivity is relatively low, the boundary radiance is dominated by thermal radiation. At shorter wavelengths the solar component dominates in both terms due to the strength of the solar radiance, the weak thermal radiance, and the increasing surface reflectivity. The contribution of the boundary radiance to the TOA signal is determined partly by the surface-to-instrument transmittance $\tau(\nu, h_s)$, which in turn depends on the absorbing gas total column. In contrast, the derivative in the second term of Equation [1] is sensitive to the height distribution of the gas species of interest. As a result, measurements performed in the shortwave channels provide information on gas total column; measurements in the longwave channels give profile information.

3.1.3 The CO Thermal Channels

The CO channel near 4.7 μm lies within the wavenumber interval $[2120, 2220]$. The instrument passband is approximately a Butterworth filter and is non-zero across most of the R-branch of the CO fundamental band. This band lies at the shortwave end of the terrestrial thermal emission spectrum. The MOPITT gas correlation technique serves to make the instrument particularly sensitive to the component of the total channel signal from the gas being measured, and allows high effective signal-to-noise. However, there is a contaminating signal due to bands of other gases in this spectral region, particularly H_2O, CO_2, O_3, and N_2O as illustrated in Figure 2 of Pan et al. [1995]. This contamination can be reduced by careful passband choice.

Since MOPITT makes a nadir measurement the Earth's surface is always in the instrument field of view. The surface provides the majority of the signal measured by MOPITT because relatively weak, optically thin, tropospheric bands are used. It is therefore important to accurately characterize the surface temperature and emissivity. The TOA radiation near 2140 cm^{-1} for a nadir view is shown in Figure 3 of Pan et al. [1995]. The gas signatures appear in absorption because the atmospheric layers are colder than the surface. The reflected downward radiance is, however, not negligible. For a daytime measurement, this reflected radiance is mainly the transmitted sunlight, while for a nighttime measurement the downward radiance is the thermal emission of the lower atmosphere. These are components of the radiance boundary term shown in Equation [2].

3.1.4 The CO and CH_4 Solar Channels

The CO and CH_4 shortwave channels use reflected solar radiation for the total column retrieval. The CO channel spans the R-branch of the first overtone CO band (0-2) at 2.3 μm, in the wavenumber interval $[4225, 4350]$. This band is relatively weak; signal-to-noise considerations and the effect of contaminating gas absorption from H_2O and CH_4 are important.

The CH_4 shortwave channel lies in the wavenumber interval $[4275, 4550]$ and covers several bands. This is a relatively clean channel with only weak interference from H_2O, CO_2, and N_2O. Figure 4 of Pan et al. [1995] shows the spectral transmittance of the optically active gases in this region. Figure 5 of Pan et al. [1995] shows the nadir atmospheric radiance with the reflected solar radiation modified by atmospheric absorption. In these passbands the signals are dominated by reflected solar radiation, the second term on the right in Equation [2]. In this case Equation [1] takes the approximate form

$$I(\nu, h) = I_o(\nu)\tau(\nu, h_s)r_s \tag{3}$$

where r_s=$(1 - \epsilon)$ is the surface reflectivity, $I_o(\nu)$ is the solar radiance, and $\tau(\nu, h_s)$ is the total transmittance along a slant path from the top of the atmosphere down to the surface at the solar zenith angle θ_{sun}, followed by an upward path to the instrument (at altitude h) along the satellite viewing angle θ_{sat} (all angles measured with respect to nadir). Assuming plane-parallel geometry, the transmittance is a function of the gas mixing ratios $\{q_n(z)\}$ and absorption coefficients $\{k_n(\nu, z)\}$, along with the dry air density $\rho(z)$, such that

$$\tau(\nu, h_s) = \exp\{-\int_{h_s}^{h} dz'(\sec\theta_{sun} + \sec\theta_{sat})\rho(z')\sum_n k_n(\nu, z')q_n(z')\} \tag{4}$$

where the summation is over all n contributing absorbers.

3.1.5 The Atmospheric Model

The atmosphere used by the forward model is divided into layers for the radiative transfer calculation. The layers lie between fixed model boundaries at 1060 hPa and 0.2 hPa. In this layering the pressure change varies with height, from 20 hPa across each layer in the lowermost troposphere to 50 hPa near the tropopause. Higher, the pressure change decreases as the 0.2 hPa upper boundary is approached. Each layer is considered homogeneous for the transmittance calculation, with a temperature and pressure given by Curtis-Godson absorber-weighted means. The integration over the total atmospheric absorption path then becomes a summation over the constituent layers. Atmospheric state parameters and the distributions of the gas constituents are constructed from climatological or meteorological data sources.

The lower boundary surface is assumed to be Lambertian. That is, reflected radiation is assumed to be unpolarized and isotropic, and is independent of the initial state of polarization and incident angle. Under these assumptions the surface is described radiatively by a Planck function having a specified temperature and an emissivity assumed constant over each MOPITT passband.

The forward model atmosphere is plane-parallel, with the exception that a spherical-earth correction is applied in each plane-parallel layer to calculate a layer-dependent zenith angle used in the radiative transfer. This MOPITT-specific parameterization leads to modifications in expressions such as Equation 4, where θ_{sun} and θ_{sat} are no longer constants but instead functions of altitude z'. A complete description of the spherical-earth correction algorithm is presented in [Edwards and Francis, 2000].

3.1.6 The MOPITT Forward Model Hierarchy

The MOPITT fast forward model is a central component of the operational MOPITT retrieval algorithm. The main challenge facing development of a fast model is the conflict between the requirements for both high accuracy and high speed. Forward model accuracy requirements are constrained by the specified accuracy and precision requirements of the MOPITT science data products. The computational speed requirement is constrained by the need to efficiently process the large number of MOPITT data measurements per orbit and the iterative nature of the optimal-estimation retrieval algorithm, which calls the forward model repeatedly during each retrieval.

Line-by-line calculations can provide high accuracy but are orders of magnitude too slow for operation use. A useful fast model must be developed along different lines, with the required speed generally obtained at some acceptable compromise in accuracy. There are also practical but very important considerations that concern efficiently designing, coding, and testing the fast model algorithm and software. These overall requirements are handled through development of a MOPITT forward model hierarchy. The hierarchy is based on the line-by-line radiance and transmittance model GENLN3. The line-by-line calculations provide a foundation for higher-level forward model algorithms culminating in the operational fast model.

Specifically, GENLN3 is used to construct an intermediate-level forward model (MOPABS) based on pre-computed absorption coefficient lookup tables. MOPABS provides accurate channel radiances, a flexible physically-based design, and a simple user interface. It runs much faster than comparable GENLN3 calculations. The operational fast model MOPFAS is a linear regression algorithm based on pre-computed datasets obtained using MOPABS.

The following three sections discuss GENLN3, MOPABS, and MOPFAS in more detail.

3.1.7 GENLN3: The Line-by-Line Radiative Transfer Model

Radiative transfer calculations are carried out using the GENLN3 line-by-line (LBL) transmittance and radiance model [Edwards and Francis, 2017]. It is based on the earlier model GENLN2 developed at Oxford University and NCAR [Edwards, 1992]. The algorithm has been designed for speed of computation, and its modular structure serves as a basis for future modification and expansion. Calculations are performed for a multi-layered atmosphere of mixed gases, and several different viewing geometries are available. Optimal atmospheric layers are calculated and refraction and spherical geometry are considered when appropriate. Several line shapes and continuum absorption are available. A two-stage spectral calculation is performed for regions close to and far from line center and there is a full treatment of line wings and of lines lying outside the spectral range of interest. Spectral line parameters are currently taken from the 2012 edition of the HITRAN database [Rothman et al., 2013]. The modeling of gas correlation spectroscopy requires accurate spectral line parameters. Spectral data for the first overtone band of CO was recalculated for the 2012 HITRAN database. Updates were made to line strengths, air- and self-broadened half-widths, the half-width temperature dependence, and pressure-induced line shifts. Line parameters for the CO fundamental band have remained unchanged for several decades. The transition frequencies for the fundamental and first overtone CO bands have not changed.

HITRAN 2012 also provides a very significant update for CH_4: over 70% of the transitions have been replaced. In particular new CH_4 data are included for lines of interest in the MOPITT CO and CH_4 NIR bands. The D-signals are in general much more sensitive to the accuracy of the line data than the A-signals because a greater part of the D-signal comes from the position of the correlation line itself. Assuming the same spectral line data is used to model both the lines of the atmosphere and the lines of the correlation cell, then there is some compensation for uncertainties in line width and almost total compensation for uncertainties in line position. The latter is important only to the extent to which the overlap with lines of the interfering species changes. The calculation of MOPITT signals is most sensitive to the accuracy of the line strength data. This has the biggest effect on the high pressure LMRs that play a role in making total column measurements and provide profile information in the lower troposphere.

In GENLN3, gas absorption other than H_2O is modeled with the Voigt line shape. Water vapor absorption is modeled using the line shape of Clough et al. [1980] to account for non-Lorentzian line wings and the water vapor continuum. GENLN3 line wings have a cutoff at 25 cm^{-1} from line center. At greater distances, the absorption is modeled using a precomputed continuum calculated from all lines and their appropriate line shape. GENLN3 uses two calculation grids. The spectral interval of interest is first divided into so-called "wide meshes" each with a typical width of 1 cm^{-1}. Each wide mesh is then sub-divided to give a high-resolution "fine" wavenumber grid. This fine grid spacing is chosen to adequately sample narrow Doppler-broadened lines in the upper atmosphere. The far-line

wing and continuum absorption, which change slowly with frequency, are calculated at three points within each wide mesh interval and then interpolated onto the fine grid. The calculation of spectral line absorption close to line center, which changes rapidly with frequency, takes place on the fine grid. This high resolution spectroscopic calculation is essential for precision MOPITT instrument modeling. Although the instrument measures integrated radiance over each passband, the gas correlation cells in front of the radiometers create a spectral response that filters the radiance at very high spectral resolution. Along with providing benchmark references, these GENLN3 calculations are the foundation for the intermediate forward model MOPABS discussed below.

3.1.8 MOPABS: The Absorption Lookup Table Forward Model

MOPABS [Edwards et al., 1999] is a crucial component of the MOPITT forward model hierarchy. It is a fast and accurate physically-based radiative transfer model upon which the efficient development of the operational fast model (MOPFAS) is based. In principle, LBL calculations could be used directly to develop MOPFAS but this is a very inefficient, albeit accurate, strategy. MOPABS, in contrast, is orders of magnitude faster relative to comparable GENLN3 calculations while retaining comparable accuracy. To accomplish this, the MOPABS calculation makes use of pre-computed line spectra created by GENLN3. These spectra include monochromatic absorption coefficients covering the channel passband intervals, as well as correlation cell A-signal and D-signal filter profiles. The MOPABS algorithm is formulated to explicitly retain the physics of the radiative transfer. As a result, the calculation can be readily modified or enhanced for related modeling studies or code improvements. For example, developing MOPFAS required an iterative approach that necessitates the computational speeds and ease-of-use obtained with MOPABS. As another example, MOPABS has proven extremely helpful as an efficient stand-alone tool to model changes in the MOPITT instrument as onboard conditions have changed in time, either due to short-term transient events or the slow alteration of optical components since launch.

3.1.9 MOPFAS: The MOPITT Fast Forward Model

Although MOPABS is accurate compared to LBL calculations, and much faster, it is nonetheless not fast enough to be used for large-volume operational CO retrievals. The MOPFAS forward model achieves sufficient operational speed and accuracy though a parameterization of wavenumber-dependent aspects of the radiative transfer physics. In particular, MOPFAS avoids an explicit time-consuming calculation of band-integrated transmittances built up monochromatically. Instead, these band-transmittances are obtained rapidly using pre-computed least-squares regression coefficients that relate the transmittances to a suite of atmospheric predictors. This regression model was developed using the computational speed and flexibility of MOPABS. Using a regression, which has good accuracy compared to LBL and MOPABS, requires a mathematical formulation of the radiative transfer in MOPFAS that is less physically explicit. Much of the physics is, in effect, buried in the regression. This is of no consequence for operational processing, but it limits the flexibility of MOPFAS for other immediate applications, which again highlights the importance of the intermediate model MOPABS.

For the MOPITT CO channels in the TIR and NIR, the MOPFAS regression training set consists of 116 atmospheres containing profiles of CO, CO_2, O_3, N_2O, and CH_4. These were constructed from a combination of model output and experimental data, and are representative of a diverse set of atmospheric states. Three separate regression calculations are carried out: one for CO transmittances (the "target gas"), the second for H_2O (the "variable gas"), and the third for the remaining contaminants (the "fixed gases"). The transmittances for these three components are defined so that their simple product gives the total channel transmittance. The atmospheric predictors, which are related to the transmittances through the regression, are various quantities involving layer temperatures, pressures, and gas amounts. Their specific choice involved both physical insight and a certain amount of trial and error to achieve sufficient accuracy in the channel radiances. Ten predictors are used for the target gas, twelve for the variable gas, and eight for the fixed gases. The approach here uses the OPTRAN

regression scheme [McMillin et al., 1995a,b]. A full description of MOPABS and MOPFAS is given in Edwards et al. [1999]. Rather than give further details of that description here, we instead highlight three modifications to the original formulation which are now included in the radiative transfer modeling.

First, MOPABS and MOPFAS both now use the spherical-earth transmittance correction mentioned in Section 3.1.5. This parameterization of the ray angle as a function of altitude is based on GENLN3 calculations in spherical geometry. It replaces the plane-parallel secant function typically appearing in optical depth calculations at both the satellite and solar zenith angles.

Second, MOPABS and MOPFAS now use a scaling calculation, and pre-computed radiances at a reference temperature, to accurately and rapidly estimate the variation of the Planck function across a channel passband in a given atmospheric layer, thereby avoiding time-consuming monochromatic calculations of this important quantity. A detailed discussion of this technique is presented in Edwards and Francis [2000].

Third, as mentioned above, MOPFAS uses a training set of 116 atmospheres. This is an extension of the original 58-member set, and features additional profiles with particularly high CO. Training the regression over this new ensemble results in an increase in the number of accurate MOPITT retrievals over fire regions and highly polluted urban areas.

3.1.10 The Instrument Model

The principles of Gas Correlation Spectroscopy were introduced in Section 2.4. Here we discuss additional spectral issues, as well as the method used to model the correlation spectroscopy for the MOPITT measurement.

At the center of a purely collision broadened spectral line, the PMR cell absorption for a given cell length and temperature is independent of cell pressure, and the radiometer D-response is zero. Away from the line center, the D-response rises to a maximum and then decreases, the exact form depending on the optical thickness of the gas cell. For the optically thin case, a double-maxima occurs a distance $\overline{\alpha_l}$ from line center, where $\overline{\alpha_l}$ is the Lorentz half width evaluated at the cell mean pressure. If Doppler broadening is also present, then the absorption at line center is greater during the high-pressure part of the modulator cycle and the D-response is non-zero.

For an LMR in the optically thin case, the D-response has its maximum at line center. However, the cell pressures needed for MOPITT are relatively large so that the LMR is optically thick at line center frequencies for most channels. This results in an LMR D-response function with a shape similar to the PMR.

The pressure, or length, modulation cycle used for the cell determines the part of the spectral line that is sampled. With increasing pressure in the correlation cell, the double peaks of the D-response function move outward from the line center. The lower pressure PMR D-response functions measure radiation from close to line center, while the higher pressure LMR D-filter has a maximum response in the line wing (Pan et al. [1995], Figure 7). Since the absorption of the upwelling surface radiation in the line wing takes place at lower altitudes, it is possible to derive information about the vertical CO profile by using a series of PMRs and LMRs with different pressures.

The goal of the forward model is to calculate the instrument signals under the conditions of the measurement. The signals measured by the MOPITT radiometers are the radiance at the top of the atmosphere, $I(\nu, h)$, convolved with the spectral response of the radiometer over the spectral passband $\Delta\nu$:

$$S_i^{A,D} = \int_{\Delta\nu} I(\nu, h) R_i^{A,D}(\nu) d\nu \qquad \text{i} = 1, \ldots, \text{m} \tag{5}$$

where $R_i^{A,D}(\nu)$ represents the Average or Difference radiometer response function for the ith radiometer. The radiometer response function can be written as the product of the response profile of the channel blocking filter G(ν) and the gas correlation response $H^{A,D}(\nu)$:

$$R^{A,D}(\nu) = G(\nu)H^{A,D}(\nu) \tag{6}$$

Assume now that the blocker response profile G(ν) varies very slowly over the wavenumber width of a GENLN3 wide calculation mesh interval of width $\delta\nu$. If there are N wide mesh intervals $j = 1, ...N$ which need not have equal spacing, then Equation 5 can be written

$$S_i^{A,D} = \sum_{j=1}^{N} \overline{G_j} \int_{\delta\nu_j} I(\nu, h) H_i^{A,D}(\nu) d\nu \tag{7}$$

where

$$\overline{G_j} = \frac{1}{\delta\nu_j} \int_{\delta\nu_j} G(\nu) d\nu \tag{8}$$

Figure 8 of Pan et al. [1995] shows the functions G(ν) and $H^D(\nu)$ for the MOPITT 4.7 μm CO thermal channel PMR. Also shown is the resultant spectrum when the response function is convolved with the atmospheric radiance. The instrument signal is then the integral of this spectrum over the channel blocker response.

The PMR or LMR cycle is modeled as a linear combination of K gas cells, each containing the correlation gas. In the PMR case, each cell has the same length but the pressure and possibly the temperature differ according to the point that the cell represents on the modulation curve. With the LMR, the signal alternates between just two gas cells of different length, with the pressure held constant. The gas correlation response is then approximated as a weighted linear combination of the monochromatic transmittances of each cell

$$H^{A,D}(\nu) = \sum_{k=1}^{K} a_k^{A,D} \tau_k(\nu)^{cell} \tag{9}$$

where $\tau_k(\nu)^{cell}$ is the transmittance of cell k and $a_k^{A,D}$ is a weighting coefficient. In this way, a two-cell approximation is modeled by setting $K = 2$. Cell 1 is the high pressure or longer cell with $a_1 = -1$ for the PMR and LMR, respectively, and cell 2 is the low pressure or shorter cell with $a2 = +1$. The gas correlation D-response in this case is

$$H^D(\nu) = \tau_2(\nu) - \tau_1(\nu) \tag{10}$$

The two-cell A-signal calculation is modeled by setting $a_1 = a_2 = 0.5$ with the same cell transmittances as in the D-signal case above. The measured pressure and temperature variations within the PMR cell can be modeled by defining cells with appropriate weights, at various times along the cycle with the corresponding temperature, pressure and gas amount.

The gas correlation response function $H^{A,D}(\nu)$ depends on the pressure or length cycle of the PMR or LMR and the temperature cycle. Thus, the same function will be applicable to many atmospheric radiance calculations that use the same PMR or LMR. The approach taken in GENLN3 is to pre-compute $H^{A,D}(\nu)$ for a particular PMR or LMR on the GENLN3 fine wavenumber grid and to store the result in a file for subsequent atmospheric calculations to use. This avoids duplication of cell transmittance calculations and makes a more accurate PMR representation possible using a larger number of composite cells. Eight cell states are used to model a PMR cycle.

3.1.11 Post-Launch Instrument Changes

Certain assumptions in the forward model design have been reexamined and updated since launch, given the length of the ongoing MOPITT mission. This has resulted in more accurate modeling and improved retrievals.

First, routine instrument telemetry indicates that the pressure and temperature of the gas correlation cells onboard MOPITT have changed with time (Worden et al. [2014], Figure 2). These changes

are now incorporated into MOPFAS by including a time-variation in the pressure and temperature of the modeled cells. In MOPFAS, LMC pressures and temperatures are updated monthly using mean values derived from recent telemetry. The PMC pressure and temperature are updated annually using values inferred from the yearly hot calibration and decontamination event.

Second, the MOPFAS regression calculation, as originally designed, involved a partitioning of relevant gases into three categories: "fixed", "target", and "variable". In this framework, the fixed gas profiles never change. In contrast, the target gas (CO or CH_4) is altered repeatedly during the retrieval iterations. The single variable gas (H_2O) is in general a function of location and time, but is held constant for a given retrieval. There are three fixed gases in the CO thermal channels: CO_2, O_3, and N_2O. In the CO shortwave channels CH_4 is the single fixed gas. In the CH_4 shortwave channels N_2O is the single fixed gas.

The fixed gas assumption is reasonable provided those gases have sufficiently small optical depth in the MOPITT passbands, or overlap weakly with MOPITT CO and CH_4 lines. However, global mean atmospheric N_2O has increased from about 315 ppbv in 1999 to 330 ppbv in 2016, a 5% increase over the MOPITT mission to date [Hall et al., 2007]. This increase, together with the presence of numerous N_2O lines in the CO thermal passband, undermines the fixed gas assumptions mentioned above. The forward model framework has therefore been modified to retain N_2O formally as a fixed gas but to slowly increase its concentration on a monthly basis. This has resulted in the following improvements in MOPITT data quality for Version 7 compared to Version 6: 1) improved mean retrieval bias and scene-dependent bias (with a few exceptions); 2) improved latitudinal dependence of bias in the middle and lower troposphere, though degraded slightly in the upper troposphere; 3) slightly improved (i.e. reduced) long-term drift for V7T (TIR-only) and V7J (joint TIR-NIR) retrievals though degraded for V7N (NIR-only) retrievals (-0.3%/yr). The fixed gas assumptions remain valid for CO_2 and O_3 in the CO thermal passband despite the significant increase in atmospheric CO_2 during the mission: no alteration of CO_2 or O_3 in MOPFAS is needed. The fixed gas assumption in the CO shortwave channel is currently under investigation, given the increase in global CH_4 and the large number of CH_4 lines near 2.3 μm. This may prove relevant to the long-term drift noted above in the V7N retrievals.

3.2 Cloud Detection and Filtering Algorithm

Mokhov and Schlesinger [1994] compared cloud climatologies from several satellite cloud measurement campaigns (ISSCP, METOR I, METEOR II, and NIMBUS 7) and surface based campaigns (BEST, WEA). They concluded that mean global cloudiness ranges from 52 to 62.5%, being slightly higher in the Southern Hemisphere. Rossow and Schiffer [1999], in a cloud climatology study for the 1986-93 period, found the global cloud amount to be ∼68%. In two separate multi-year studies of HIRS data (of horizontal resolution very similar to that of MOPITT), Wylie et al. [1994] and Wylie and Menzel [1999] found that only ∼25% of observations were cloud free. As shown by these and other studies, clouds are globally pervasive.

Clouds impact the radiation measured by MOPITT at 2.2, 2.3, and 4.7 μm, hindering the gas retrieval process. Identifying and discarding observations affected by clouds is, thus, crucial. MOPITT retrievals are obtained from cloud-free observations; retrievals are also produced under certain circumstances if low clouds are present, since MOPITT radiances are less sensitive to the portion of the atmosphere close to the surface, and hence, to low clouds. The clear/cloudy status of an observation is determined from both MOPITT thermal-channel radiances and simultaneous measurements from MODIS (the MODerate resolution Imaging Spectroradiometer), also onboard the Terra platform.

3.2.1 Physics of the Problem: Cloudy Sky Radiance

The interaction of solar radiation and thermal emission with clouds is a function of the cloud particle characteristics. Optical thickness and effective radius are often used to describe how incident radiation reacts with a cloud and to evaluate empirical measurements with theoretical models. Optical thickness is determined by the wavelength of incident radiation, physical nature of the particles (ice crystals,

drops, droplets), their concentration, and the vertical extent of the cloud. The effective radius r_e is defined as [Hansen and Travis, 1974]

$$r_e = \int r^3 n(r) dr / \int r^2 n(r) dr \tag{11}$$

where r is the particle radius, and $n(r)$ the particle size distribution.

King et al. [1990], Nakajima and King [1990], and Nakajima et al. [1991] evaluated the reflectance of water clouds as a function of optical thickness and effective radius in the solar reflected infrared (or near infrared). Their results show that in the range where the MOPITT near infrared bands are located, cloud reflectance increases with increasing optical thickness; it decreases with larger particle sizes due to moderate absorption by water. Ice particles produce, roughly, similar effects [Irvine and Pollack, 1968].

In the thermal infrared, the distinction between a cloud and its underlying surface is due not only to the reflectance properties of the cloud but also to the cloud's thermal emission. Hansen and Pollack [1970] showed that in liquid water clouds (warm clouds) the thermal emission factor dominates, while ice clouds (cold clouds) can have equal contributions of thermal emission and solar reflectance. Observations in the thermal infrared are also sensitive to thermal emission through semi-transparent clouds, resulting in a reduction of surface contrast and increased difficulty in determining the presence of optically thin clouds.

The presence of clouds introduces additional terms in Equation [1] and associated complexities in retrieving CO. Radiation reaching the instrument will contain not only radiation from the surface and atmosphere, but from one or more levels of clouds that may cover only part of the field of view. It may be possible to carry out retrievals over a solid, opaque layer with a well-defined top that fills the FOV, but this is not now part of the retrieval algorithm. The problems created by unknown or imperfectly known cloud heights and their variations as well as spatially varying cloud properties will need to be solved before this becomes a reality.

Broken clouds, or non-opaque clouds, will result in radiation from clouds as well as the surface reaching the instrument, with differing atmospheric columns and amounts of CO. Here the large problems are fractional fields covered, as well as the problems of uncertain cloud heights, opacities and scattering characteristics, for which there does not appear to be enough independent information to obtain solutions.

For these reasons, MOPITT retrievals are not attempted in FOVs that have more than a small amount of detected cloud, unless these are identified as low clouds.

3.2.2 Identification of MOPITT Clear/Cloudy Observations

MOPITT radiances are evaluated by applying a threshold test; the result is a MOPITT clear/cloudy assignment for each observation. All MOPITT pixels are re-evaluated using Terra-MODIS cloud mask data. Information from both datasets is utilized to make a final identification of MOPITT cloudy observations, which are then not further processed.

3.2.2.1 The MODIS Cloud Mask Terra-MODIS [King et al., 1992] acquires data in 36 spectral bands in the visible and infrared regions of the spectrum. The MODIS cloud mask algorithm [Ackerman et al., 2010] applies a series of visible and infrared threshold and consistency tests to determine if observations are clear or obstructed (by clouds, aerosols). MODIS cloud mask products (Ackerman et al., 2015; dx.doi.org/10.5067/MODIS/MOD06_L2.006) are generated at 0.25 km to 1 km horizontal resolution at nadir, the former based on visible information only.

The MODIS viewing swath amply contains that of MOPITT (2330 and 640 km, respectively). Each MOPITT observation coincides with a number of simultaneously acquired MODIS observations (∼484). Thus, the Terra-MODIS cloud mask interprets the signal from the same atmospheric and surface conditions as the MOPITT instrument, albeit on a much finer scale.

V7 is the first MOPITT release to use exclusively MODIS cloud mask products from collection 6 [Lyapustin et al., 2014]. MOPITT V5 and V6 used MODIS collection 5 products [Lyapustin et al., 2014] until February 2016 and collection 6 products starting in March 2016.

3.2.2.2 MOPITT-MODIS Co-location MOPITT and MODIS data are spatially and temporally co-located in a two-step process which is repeated for each MOPITT track. (A track is a set of 29 stares acquired during the instrument's back and forth scanning motion. Each stare is composed of 4 pixels, each of them ∼22x22 km^2 at nadir, arranged along the satellite's path. See Figure 3 for details.) In the first step of the co-location, a 0.04°x0.04° (∼4.5x4.5 km^2) search box is defined around the center of the MOPITT track. (The coordinates of the track's center are the average of those of pixels 2 and 3 in stare 22, or pixels 1 and 4 in stare 22, or pixels 2 and 3 in stare 21, or pixels 1 and 4 in stare 21, depending on availability.) Then, all the MODIS pixels inside the search box are gathered and the closest to its center ("MODIS central") is singled out. In the second step of the co-location, all MODIS pixels inside a MOPITT pixel ("insiders") are identified; how this is achieved varies depending on the MOPITT version, but it is always based on the fact that the relative location and viewing angle of the two instruments are fixed.

In MOPITT V4 and older the second step of the co-location was performed via parametrization. For each MOPITT pixel, the insider MODIS pixels were identified based on their location in the MODIS granule with respect to MODIS central, by applying a set of empirically-derived equations tailored to fit each MOPITT pixel in a track.

In MOPITT V5 and following the second step was modified to use a single set of location indices to identify the MODIS insider pixels relative to the location of MODIS central. These indices are neither time- nor location-dependent; thus, they can be used for each MOPITT pixel in any track in the dataset. This method is faster and more accurate than the parametrization-based method, resulting in both more MODIS insider assignments and less miss-assignments.

3.2.2.3 Clear/Cloudy Assignment After co-location, relevant cloud mask parameters of the MODIS insiders (listed in Table 2) are gathered and averaged for each MOPITT pixel. The averaged values are stored in the MODIS Cloud Diagnostics field in MOPITT L2 files of V5 and later.

The set of rules summarized in Table 3 is applied to the MODIS- and MOPITT-only assignments, and a final clear/cloudy decision is reached for each MOPITT pixel; cloudy pixels are not further processed. Cloud descriptor values are available in the Cloud Description field in MOPITT L2 files.

MOPITT cloud detection is based on the fact that clouds are generally colder and, thus, have lower emission than the underlying surface. For each MOPITT observation (i.e., pixel), the radiance measured by one of the 4.7 μm thermal channels (1A for Phase 1, 7A for Phase 2) is compared to the a priori clear-sky radiance calculated by MOPFAS. (Thermal emission radiances are used because, unlike solar-reflected radiances, they can be measured both during daytime and nighttime.) If the measured/calculated ratio is above a 0.955 empirical threshold the observation is considered clear. However, under temperature inversion conditions, such as when surface radiative cooling is very high, clouds may be warmer than the underlying surface, resulting in very high ratio values. Because of this, the threshold method is only applied to observations equatorward of latitude ±65°.

A MODIS "clear" value is assigned to any given MOPITT pixel if <5% of its "insider" MODIS pixels are found to be cloudy. This threshold was chosen because, according to Warner et al. (internal report), it results in clear/cloudy MOPITT ratios similar to those observed in global climatological studies [Wylie et al., 1994; Wylie and Menzel, 1999]. When a MOPITT pixel is assigned a MODIS "clear" value and a MOPITT "cloudy" value, the former supersedes the latter.

For daytime observations, an averaged MODIS IR threshold test value ≥0.9 and an averaged MODIS visible reflectance test value ≤0.95 are interpreted as low clouds. For nighttime observations a MODIS IR temperature difference test value ≥0.9 is interpreted as low clouds. When low clouds are identified, the result of the MOPITT radiance test determines if the MOPITT pixel is ultimately clear over low clouds or cloudy.

Due to electronic crosstalk affecting some of the Terra MODIS thermal channels since 2010 [Sun et al., 2015, 2016], Terra MODIS cloud mask products of collections 5 and 6 show a false trend towards increasing cloudiness, particularly for tropical scenes over the ocean. To address this issue, a new descriptor value "6" was added in MOPITT V7.

3.3 Retrieval Algorithm for CO

MOPITT CO retrieval products have been refined continuously since the launch of TERRA [Worden et al., 2014]. Major changes to the retrieval algorithm have included the sources of CO a priori information and meteorological data, and the retrieval grid. Significant differences in the Level 2 processing system used to generate MOPITT V3, V4, V5, V6 and V7 products are summarized in Table 4. Improvements to the retrieval products have also resulted from enhancements in (1) the Level 1 radiance product (e.g., improved geolocation data and more realistic radiance uncertainties), (2) the cloud detection algorithm (as described in Section 3.2) and (3) the fast radiative transfer model (as described in Section 3.1).

In this section we describe the retrieval method used to process MOPITT L1 radiances and review in detail all of the significant changes made to the algorithm during the operational phase of MOPITT (through 2016). A nonlinear optimal estimation algorithm [Rodgers, 2000; Pan et al., 1998] and a fast radiative transfer model [Edwards et al., 1999] are used to invert the measured Average and Difference radiances to determine the CO vertical profile. In general, retrievals of CO may involve up to six channels in two distinct bands: two LMC-based channels in a solar reflectance band near 2.3 μm (Channels 2 and 6), two LMC-based channels in a thermal emission band near 4.7 μm (Channels 1 and 5) and two PMC-based channels in the 4.7 μm band (Channels 3 and 7). Only clear-sky radiances (i.e., radiances uncontaminated by clouds) are processed by the retrieval algorithm. The MOPITT cloud-detection algorithm is described in Section 3.2. Possible radiative effects from aerosols are neglected in the retrieval algorithm, since aerosols rarely have significant radiative effects in MOPITT's infrared spectral bands [Eck et al., 1999].

In addition to the CO thermal-band and solar-band channels just described, MOPITT includes two LMC-based channels for measuring methane (Channels 4 and 8). However, to date, no operational MOPITT methane product has been developed or released. Spectral variability of the surface reflectance across the methane filter passband [Pfister et al., 2005] and geophysical noise [Deeter et al., 2011] were found to be major obstacles to the development of a methane product.

3.3.1 Mathematical Formulation

3.3.1.1 Optimal Estimation In atmospheric remote sensing, the common problem of inverting a set of observations (e.g., calibrated radiances) to determine aspects of the atmospheric state (temperature profile, trace gas mixing ratio profiles, etc.) is often ill-conditioned, meaning that no unique solution exists. Thus, additional information of some type is usually required to constrain the retrieval to fall within physically reasonable limits. The CO retrieval algorithm used for MOPITT exploits the maximum a posteriori ("MAP") solution which is a specific type of optimal estimation [Rodgers, 2000]. The general strategy of such techniques is to seek the solution most statistically consistent with both the measurements and the observed patterns of CO variability as represented by the a priori. The methodology used for generating the a priori (i.e., both the a priori mean profile and the a priori covariance matrix) is described in detail in Section 3.3.2.

The equation relating the true atmospheric state and the measured radiances can be written as

$$y = F(x, b) + N_\epsilon \tag{12}$$

where y is the measurement vector (i.e., the set of observed MOPITT radiances), x is the state vector (i.e., the set of all desired retrieved variables), b represents all other forward model parameters (i.e., all parameters needed to calculate the MOPITT radiances not explicitly included in the state vector), $F(x, b)$ represents the forward radiative transfer model [Edwards et al., 1999], and N_ϵ is the radiance

error vector. The purpose of the retrieval algorithm is to estimate the most probable true state vector x consistent with the measured radiances y and the associated measurement errors.

In the MOPITT CO retrieval algorithm, the measurement vector y is formed solely from the calibrated satellite radiances. For the thermal-band channels (1, 3, 5, and 7), S_i^A and S_i^D are used to represent the A and D radiances for Channel i and are included in the measurement vector y directly. For the solar-band channels (2 and 6) a different strategy is employed. In this case the ratio $S_i^R = S_i^D/S_i^A$ is used because it greatly reduces the effect of the generally unknown and highly variable surface reflectivity; both S_i^D and S_i^A are directly proportional to the surface reflectivity. The D/A ratio is a useful measurement for retrieving CO because of the much greater sensitivity to CO exhibited by S_i^D compared to S_i^A. Forward model studies also indicate that the contaminating effects of gas species other than CO are reduced in the ratio S_i^R [Pan et al., 1995]. For these reasons, the solar-band channels are represented in y through the solar ratio signal S_i^R.

The thermal-band radiances depend not only on the atmospheric CO distribution but also on the atmospheric temperature and water vapor mixing ratio profiles, as well as the surface temperature T_{sfc} and surface emissivity ϵ_{sfc}. Accurate values for all of these geophysical parameters are necessary to produce useful CO retrievals. Sources of reanalysis data are insufficient for providing accurate values of surface temperature and emissivity (both of which are highly variable) at the temporal and spatial resolution corresponding to individual MOPITT observations. Fortunately, information contained in the MOPITT thermal-band radiances allows retrieval of the surface temperature and emissivity along with the CO profile, and makes external data sources for these quantities necessary only for providing a priori values (Section 3.3.2.3).

Thus, rather than assuming fixed values for T_{sfc} and ϵ_{sfc}, both parameters are included in the retrieval state vector x along with the elements of the CO profile. (A detailed inspection of the radiative roles of T_{sfc} and ϵ_{sfc} reveals that their effects on the thermal-band radiances are often similar. Therefore, MOPITT radiances do not necessarily contain sufficient information to retrieve both parameters independently. Both parameters are included in the retrieval state vector because (1) they represent physically different sources of radiance variability and (2) assuming fixed values for either parameter would unnecessarily constrain the CO retrieval.)

The general measurement and state vectors for a given observation can be written as:

$$y = (y_i) = \left\{ \begin{array}{c} S_1^A \\ \vdots \\ S_4^A \\ S_1^D \\ \vdots \\ S_4^D \\ S_1^R \\ S_2^R \end{array} \right\} \tag{13}$$

and

$$x = (x_j) = \left\{ \begin{array}{c} \epsilon_{sfc} \\ T_{sfc} \\ q_1 \\ q_2 \\ \vdots \\ q_n \end{array} \right\} \tag{14}$$

where q_j represents the CO mixing ratio at the j'th pressure level of the predefined retrieval grid.

The MAP solution effectively combines state vector estimates determined from (1) the measurement vector y and (2) the "virtual" measurement represented by the a priori state vector x_a, inversely

weighted by their respective covariances. The MAP solution $\hat{x}$ is thus written

$$\hat{x} = (C_a^{-1} + K^T C_\epsilon^{-1} K)^{-1} (C_a^{-1} x_a + K^T C_\epsilon^{-1} y) \tag{15}$$

where C_a is the a priori covariance matrix, K is the weighting function matrix (or "Jacobian"), K^T is its transpose, and C_ϵ is the radiance-error covariance matrix. K describes the model-calculated sensitivity of each of the measurement vector elements to each of the elements of the state vector and is defined by

$$K_{ij} = \frac{\partial F_i}{\partial x_j}. \tag{16}$$

As developed in Section 3.3.3, C_ϵ represents radiance errors and error correlations from sources including instrumental noise, geophysical noise, and forward model error. The corresponding retrieval error covariance matrix for the MAP solution is

$$C_{\hat{x}} = (C_a^{-1} + K^T C_\epsilon^{-1} K)^{-1} \tag{17}$$

and describes the uncertainties and correlations in the retrieved state vector $\hat{x}$.

Equation 15 for the MAP solution can not be used directly to retrieve the CO profile because the weighting function matrix K is itself a function of $\hat{x}$. Therefore, an iterative form of the MAP solution is needed. The method of Newtonian iteration, in which

$$\hat{x}_{n+1} = x_a + C_a K_n^T K_n C_a K_n^T + C_\epsilon{}^{-1} [y - F_n - K_n (x_a - \hat{x}_n)] \tag{18}$$

where n is the order of iteration, and F_n is the theoretical radiance vector based on $\hat{x}_n$ as calculated by the forward model, is therefore exploited [Rodgers, 2000]. Generally, the initial guess state vector $\hat{x}_0$ is set to the a priori state vector x_a which is described further in Section 3.3.2.1. After each iteration of the MAP solution, the solution is checked for convergence. The convergence test is based on the fractional change in the CO profile relative to the previous iteration. Iterations cease when the root-mean-square (RMS) value of the CO fractional change (over the entire profile) decreases to 5% or less. In practice, retrievals typically converge within four iterations. Experience with the processing of actual MOPITT data demonstrates that increasing the number of retrieval iterations (i.e., decreasing the convergence threshold) produces a negligible effect on the retrieval results.

3.3.1.2 Log(VMR) State Vector Whereas the state vector in the original Version 3 retrieval algorithm represented the CO vertical profile as a set of VMR values, the state vector used for all newer products represents the CO profile as a set of log(VMR) values. Motivations for this change (based on in-situ analyses) and its consequences with respect to the retrieval algorithm are detailed in Deeter et al. [2007]. For simplicity, the operational retrieval software relies on base-10 logarithms for log(VMR) calculations; however, the use of natural logarithms would produce identical retrieved VMR values. Long-term observations in diverse locations demonstrate that the log-normal model represents the variability of tropospheric CO concentrations better than the VMR-normal model. VMR-based and log(VMR)-based state vectors imply fundamentally different a priori constraints and can lead to retrievals with substantially different characteristics. Benefits of the log(VMR)-based model for CO profile retrievals include improved retrieval convergence and fewer retrievals with unrealistically small VMR values [Deeter et al., 2010].

3.3.1.3 Retrieval Grid and Layering Scheme Retrievals of the CO vertical profile consist of a "floating" surface-level retrieval (tied to the pixel-dependent local surface pressure value) and retrievals for a set of fixed pressure levels. For the original V3 product, the fixed levels included 850, 700, 500, 350, 250, and 150 mb. In all newer product versions, the retrieval algorithm has exploited a ten-level retrieval grid including levels at the surface, 900, 800, ... and 100 hPa. In elevated regions where one or more of the fixed pressure level values exceed the actual local surface pressure, the

retrieval is performed on a grid consisting of the local surface pressure and the appropriate subset of fixed pressure levels with pressures less than the surface pressure.

Internally, the MOPITT retrieval algorithm assumes a defined relationship between (1) VMR values at the fixed retrieval grid levels, which are reported as the retrieved CO profile, and (2) VMR values at pressure levels within the layers spanning adjacent grid levels. This assumed level/layering relationship was modified for the V5 retrieval product and has not changed for subsequent product versions. According to the new level/layering scheme, each retrieval level corresponds to the layer immediately above that level. Within each such layer, the VMR is assumed constant. For example, the VMR retrieval product for 700 hPa actually corresponds to the mean VMR for the layer between 700 and 600 hPa. The surface-level VMR retrieval product actually corresponds to the mean VMR for the layer between the surface and 900 hPa (assuming the surface pressure exceeds 900 hPa). The topmost retrieval level represents the layer between 100 and 50 hPa. In contrast, the layering scheme used for V3 and V4 products employed non-uniformly weighted layers [Deeter et al., 2009].

3.3.1.4 Retrieval Averaging Kernels The concept of the retrieval averaging kernel [Rodgers, 2000] is fundamental to understanding the physical significance of the retrieved MOPITT CO profile. The averaging kernel A describes the dependence of the retrieved state vector $\hat{x}$ on the true state vector x through the relation:

$$A = (\frac{\partial \hat{x}}{\partial x}). \tag{19}$$

For the MAP retrieval algorithm employed for MOPITT retrievals, the retrieved state vector $\hat{x}$ can be expressed as a weighted average of the true state vector x and a priori state vector x_a through the relation

$$\hat{x} \approx Ax + (I - A)x_a \tag{20}$$

where I is the identity matrix.

A is related to the retrieved error covariance matrix C_x and the fixed a priori covariance matrix C_a through the relation

$$A = I - C_x C_a^{-1}. \tag{21}$$

In the ideal case, A would equal I, and any perturbation to the true state vector would produce identical changes in the retrieved state vector. Generally, however, changes to any particular element of the true state vector result in finite changes to all elements of the retrieved state vector. Analysis of the retrieval averaging kernels permits analysis of (1) the vertical resolution and sensitivity of the retrieval and (2) the degree to which the a priori information influences the retrieval.

Each row of A describes how all of the elements in the true state vector contribute to a particular element of the retrieved state vector and constitutes the averaging kernel for that element of the retrieved state vector. Averaging kernels for each level in the retrieved profile do not necessarily peak at the corresponding pressure level of the true profile. For example, the averaging kernel for the surface-level retrieval often peaks at a somewhat higher level, such as 800 or 900 hPa [Deeter et al., 2011]. This behavior is closely related to the features of the MOPITT weighting functions. Both the weighting functions and CO averaging kernels exhibit significant variability. Generally, all variables which are required as inputs to the forward radiative transfer model influence A. In particular, though, variability of the atmospheric temperature profile, surface pressure and temperature, and actual CO profile are responsible for most of the variability in the averaging kernels [Worden et al., 2013]. Examples of MOPITT averaging kernels are presented in various publications [Deeter et al., 2003, 2007; Worden et al., 2013].

For quantifying the information content of trace-gas retrievals like those of MOPITT, Rodgers showed that the "Degrees of Freedom for Signal" (or DFS) provides a simple scalar index [Rodgers, 2000]. For the MOPITT retrieved CO profiles, DFS is the sum of the eigenvalues of A, which is also the trace of A (i.e., the sum of the diagonal elements). In the context of the eigenvalues and eigenvectors of A, DFS represents the number of orthogonal components in the retrieved profile which

are retrieved with no contribution from the a priori profile [Rodgers, 2000; Pan et al., 1998]. Simply stated, DFS is a measure of the number of independent components of the retrieved CO profiles that are not constrained by the a priori. Like the averaging kernel matrix, MOPITT DFS values exhibit significant geographical and long-term temporal variability [Deeter et al., 2015].

3.3.1.5 Retrieval of CO Total Column The retrieved CO total column $\hat{c}$ is defined as the number of CO molecules per unit area (also known "vertical column density") obtained by integrating the CO number density (consistent with the retrieved VMR profile) from the surface to the top of the atmosphere. This quantity is calculated within MOPFAS. The uncertainty in the retrieved total column is obtained from the retrieval error covariance matrix $C_{\hat{x}}$ through the relation

$$C_{\hat{c}} = g^T C_{\hat{x}} g \tag{22}$$

where $C_{\hat{c}}$ is the total column error covariance (a scalar) and g is the total column linear operator which relates the profile $\hat{x}$ and the total column value $\hat{c}$ [Rodgers, 2000].

3.3.2 A Priori

In the context of the MAP retrieval algorithm, the term "a priori" refers to both the a priori state vector and the a priori covariance matrix, which represents the expected variability of all state vector elements and their correlations. A priori information is required for the CO profile, surface temperature and surface emissivity.

3.3.2.1 A Priori State Vector Except for the original V3 product, which used a fixed "global" a priori profile for all observations [Deeter et al., 2003], all MOPITT retrieval products rely on variable a priori to represent the geographical and seasonal variability of "background" concentrations of CO. For the V4 and V5 products, the a priori was based on monthly CO climatologies for the years 1997–2004 [Deeter et al., 2010] as simulated with the MOZART chemical transport model [Emmons et al., 2010]. For the V6 and V7 products, the CO a priori is based on monthly climatologies for the years 2000–2009 simulated with the CAM-Chem model [Lamarque et al., 2012]. MOPITT a priori log(VMR) values vary by month, but do not vary from year to year; this simplifies the interpretation of long-term trends in the data. For all MOPITT product versions, model-based climatologies used to generate the a priori are gridded at one degree (lat/lon) horizontal resolution and monthly temporal resolution. Spatial and temporal interpolation are used to generate a priori values at each specific observation location and day.

3.3.2.2 A Priori Covariance Matrix The a priori covariance matrix C_a consists of rows and columns for each element in the state vector, including surface temperature and emissivity. This matrix defines the applied constraint in the MAP retrieval algorithm. Variations in surface temperature and emissivity are assumed to be uncorrelated to each other and to variations in the CO profile. Thus the only non-zero elements in the rows and columns in C_a that represent surface temperature and emissivity are the diagonal elements. The remaining submatrix of the a priori covariance matrix describes the expected variability and inter-level correlations of the CO profile. Diagonal elements of this submatrix quantify the variances at each of the pressure levels in the retrieval grid. Off-diagonal elements describe correlations of CO variability for each pair of levels.

In the V3 retrieval algorithm, where the state vector represented CO in terms of VMR, the CO a priori covariance matrix quantified variability also in terms of VMR. However, for V4 and subsequent MOPITT production versions, the a priori covariance matrix describes the variability of log(VMR). Because

$$\partial(ln(VMR)) = \partial(VMR)/VMR \tag{23}$$

log(VMR) variances and covariances describe fractional (or relative) VMR variability rather than absolute VMR variability. As shown in Deeter et al. [2007], analyses of in-situ datasets for geographically diverse locations demonstrate that fractional VMR variability is more consistent (i.e., varies less from site to site) than absolute VMR variability. For example, regions which are typically unpolluted (on average) exhibit smaller VMR variances than CO source regions with greater mean VMR values. These observations, coupled with the fact that available observations and models are insufficient for developing a variable a priori covariance matrix applicable to all geographic regions in all seasons, favor the use of a single a priori covariance matrix for all retrievals. This choice also makes physical interpretation of the retrievals simpler than if a variable a priori covariance matrix were employed.

For V4 and subsequent MOPITT products, the a priori covariance matrix C_a incorporates the same variance value C^O at all levels, with a constant correlation height P^c (expressed in hPa) defining the off-diagonal elements [Engelen and Stephens, 1999]. Thus,

$$C_{a,ii} = C^0 \tag{24}$$

and

$$C_{a,ij} = C^0 \exp\left[-(p_i - p_j)^2/(P^c)^2\right] \tag{25}$$

where p_i and p_j are the pressures for retrieval levels i and j, respectively. C^0 is set to $(0.30 log_{10} e)^2$, corresponding to a fractional VMR variability of 30%, and P^c is set to 100 hPa. The relatively small value for P^c minimizes the "projection" (or extrapolation) of information from levels where the MOPITT weighting functions are relatively strong (e.g., the mid-troposphere) to levels where the weighting functions are relatively weak (e.g., the surface). While approximate, these values for C^0 and P^c are generally consistent with analyses of aircraft in-situ datasets at individual MOPITT validation sites.

3.3.2.3 A Priori Surface Temperature and Emissivity Values A priori values and variances are also required for surface emissivity and surface temperature. For the MOPITT V3 product, a priori surface emissivity values were based on a published surface emissivity database coupled to a geographical database of surface type [Deeter et al., 2003]. For all later product versions, however, a priori surface emissivity values were derived from an analysis of gridded MOPITT radiances and corresponding MODIS surface temperatures [Ho et al., 2005]. The assumed surface emissivity a priori variance for V3 was 0.025 but was decreased to 0.0025 for all later product versions. The current variance value of 0.0025 represents an emissivity uncertainty of 0.05.

For surface temperature, V3, V4 and V5 a priori values were based on spatially and temporally interpolated surface-air temperatures from the NCEP GDAS (Global Data Assimilation System) analysis. For the V6 product, a priori surface temperatures were based on interpolated "skin temperature" values included in the MERRA (Modern-Era Retrospective Analysis For Research And Applications) reanalysis. (See Section 3.3.4 below.) MERRA was then replaced by MERRA-2 for V7 processing. The assumed surface temperature a priori variance for all surface types and all product versions is 25 K^2 (corresponding to an uncertainty of 5 K), except for V7 oceanic scenes for which the a priori variance was reduced to 1 K^2.

3.3.3 Measurement Errors

3.3.3.1 Radiance Bias Corrections The MOPITT processor exploits a set of radiance L2-bias correction factors to compensate for relative biases between (1) simulated radiances calculated by the operational radiative transfer model and (2) actual calibrated L1 radiances. Without some form of compensation, radiance biases produce biases in the retrieved CO profiles. Radiance bias correction factors may compensate for a variety of potential bias sources including errors in instrumental specifications, forward model errors, spectroscopic errors, and geophysical errors. Prior to releasing new MOPITT products, final correction factors are determined iteratively, using retrieval validation results for CO retrieved profiles and total column as indicators of radiance bias. Radiance correction factors

used for all MOPITT product versions released to date are listed in Table 5. Within the retrieval processing software, radiances calculated by the operational fast radiative transfer code (MOPFAS) are scaled by the listed radiance correction factors.

For V7 products, radiance bias factors were optimized using retrieval validation results. For the TIR radiances (Channels 5 and 7), radiance bias scaling factors were determined by minimizing observed retrieval biases at 400 and 800 hPa as determined using validation results based on in-situ CO profiles from the HIPPO (HIAPER Pole to Pole Observations) field campaign [Deeter et al., 2013]. To the extent that the HIPPO campaign produced a near-global set of in-situ CO profiles (i.e., over a wide latitudinal range spanning both the Northern and Southern Hemispheres), this strategy effectively yields globally-minimized retrieval biases. For the NIR radiances (Channel 6), radiance bias scaling factors were determined by minimizing NIR-only retrieval biases as determined using the NOAA aircraft profile set. (The HIPPO dataset primarily represents oceanic scenes and was therefore not useful for optimizing the NIR radiance-bias scaling factors.)

3.3.3.2 Radiance Uncertainties The radiance error covariance matrix C_ϵ describes the uncertainties and error correlations of all elements of the measurement vector y. For MOPITT CO retrievals, C_ϵ includes components representing (1) random instrumental and geophysical noise and (2) forward model error. Thus,

$$C_\epsilon = C_y + C_f \tag{26}$$

where C_y is the radiance noise covariance matrix and C_f is the forward model error covariance matrix.

C_y is formed with non-zero elements on the matrix diagonal only, which is equivalent to assuming that only uncorrelated noise processes act on the various MOPITT thermal-band and solar-band radiances. Instrument noise measurements are performed approximately every two minutes from data acquired during periodic space-view intervals. Observations of the space-view background provide a zero-radiance reference which is useful for both radiance calibration and instrument noise characterization. For each radiance and for each of the four elements of the detector array [Drummond, 1992] the instrument noise is calculated as the product of the standard deviation of the uncalibrated instrument data (in digital "counts") acquired during these space views and a calibration gain factor which converts the value into radiance units. Finally, for each radiance and each of the four detector array elements, all instrument noise values for each day are averaged to produce a single daily noise value. (Details of the methods used to convert counts into radiances and noise values are described in the MOPITT L1 ATBD.)

Beginning with the release of MOPITT V5 products, a new method was exploited for calculating elements of C_y corresponding to MOPITT's LMC channels (i.e. 1, 2, 5, and 6) [Deeter et al., 2011]. The new method implemented in the L1 Processor accounts for both instrumental noise and "geophysical noise," i.e., random errors in the calibrated radiances resulting from the combined effects of field of view motion and fine-scale spatial variability in surface radiative properties during each observation [Deeter et al., 2011]. All earlier MOPITT retrieval products only accounted for instrumental noise. Over land, the magnitude of geophysical noise varies strongly, even for adjacent MOPITT pixels, and is often much greater than the instrumental noise. In the retrieval algorithm, the representation of both instrumental noise and geophysical noise in C_y changes the effective weighting of the radiances for each observation and yields more reliable retrieval uncertainties.

As discussed in detail in Section 3.1.6, the operational forward model MOPFAS was designed for both accuracy and computational efficiency, and therefore lacks the precision of a line-by-line model. MOPFAS is a parameterization of MOPABS, which is itself a derivative of the line-by-line radiative transfer model GENLN3. To characterize the forward-model error, a statistical analysis was made of the radiance errors between MOPFAS and MOPABS for all profiles used in the development of the MOPITT V3 a priori [Deeter et al., 2003]. Radiance error vectors were formed for each profile by regarding the MOPABS radiances y_{abs} as "truth" and subtracting those values from the corresponding MOPFAS values y. Thus, this analysis does not account for errors in MOPABS itself which, for example, might be due to errors in the HITRAN spectroscopic database. The forward model radiance

error covariance matrix was then calculated by computing the expectation value E of the vector (y - y_{abs}):

$$C_f = E\{(y - y_{abs})(y - y_{abs})^T\} \quad (27)$$

Mathematically, C_f is calculated by forming a matrix of the vector quantity (y - y_{abs}) calculated for all profiles used in the development of the a priori, multiplying this matrix by its transpose, and then normalizing by the number of profiles. Calculated this way, fractional radiance errors for the MOPITT CO channels vary from approximately 0.1 to 0.5% and exhibit substantial correlations with each other (i.e., diagonal and off-diagonal elements of C_f are generally of the same order of magnitude).

3.3.3.3 Meteorological Fields For each CO retrieval, the MOPITT retrieval algorithm requires temperature and water vapor profiles as well as a priori surface temperature values. For the V3, V4, and V5 L2 processors, relevant meteorological data were extracted from NCEP (National Center for Environmental Prediction) GDAS (Global Data Assimilation System) forecast products and then interpolated spatially and temporally to each MOPITT observation. For V6 processing, meteorological profiles were interpolated from NASA MERRA (http://gmao.gsfc.nasa.gov/merra/) [Rienecker et al., 2011]. Several benefits result from using MERRA products rather than NCEP. First, generally higher quality retrieval results are expected due to higher quality water vapor profiles; unphysical values in NCEP water vapor profiles [Deeter et al., 2013] were previously found to sometimes cause anomalous surface-level CO concentrations over the ocean offshore of California. Also, higher quality retrieval results should be achieved over land due to the use of hourly-resolved MERRA surface skin temperatures instead of six-hourly NCEP surface-level air temperatures. Skin temperature represents the radiative surface temperature to which MOPITT thermal-channel radiances respond much better than air temperature at the surface. Higher quality retrieval results are also expected due to higher horizontal and vertical spatial resolution in the meteorological fields; MERRA is produced at 1/2 by 2/3° (lat/lon) horizontal resolution on a 42-level pressure grid whereas NCEP GDAS products are produced at 1° horizontal resolution on a 26-level pressure grid. Finally, improved long-term stability of MOPITT retrieval products are expected as the result of the use of climate-quality reanalysis instead of output from a meteorological forecasting system. MERRA reanalysis products are typically released one month at a time, with a data latency of about two to three weeks. This leads to data latencies for MOPITT V6 products of one to two months and prevents their use in near-real-time applications.

For all V7 products, meteorological profiles are extracted from the MERRA-2 product (http://gmao.gsfc.nasa.gov/reanalysis/MERRA-2). MERRA-2 was introduced to replace the original MERRA dataset because of the advances made in the assimilation system that enable assimilation of modern hyperspectral radiance and microwave observations, along with GPS-Radio Occultation datasets. It also uses NASA ozone observations after 2005. Additional advances in both the GEOS-5 model and the GSI assimilation system are included in MERRA-2. Spatial resolution remains about the same (∼50 km in the latitudinal direction) as in MERRA. Generally higher quality retrieval results for V7 are expected using MERRA-2 due to the assimilation of more satellite datasets (e.g., IASI) and other improvements.

3.3.4 MOPITT Spectral Variants: TIR-only, NIR-only and TIR-NIR

As described in Section 3.3.3.1, the MOPITT L2 processor exploits a set of radiance-bias correction factors (Table 5) to compensate for relative biases between (1) simulated radiances calculated by the operational radiative transfer model and (2) actual calibrated L1 radiances. Radiance bias correction factors compensate for a variety of potential bias sources including errors in instrumental specifications, forward model errors, spectroscopy errors, and geophysical errors.

MOPITT V3 and V4 retrievals were exclusively based on thermal-band radiances. For observations made before 7 May 2001 (i.e., before the loss of Channels 1-3 resulting from a failure of one of MOPITT's coolers), V3 and V4 retrievals were based on the Difference radiances for Channels 1, 3, and 7, and the Channel 7 Average radiance. For observations made after the anomaly, all V3 and V4

retrievals were based on the Difference radiances for Channels 5 and 7, and the Channel 5 Average radiance.

After the launch of MOPITT, the main obstacle to effectively exploiting MOPITT's NIR observations was determined to be a lack of understanding of NIR radiance errors. Over land, it became evident that the combined effects of field of view motion and sub-pixel variability in surface characteristics produced random "geophysical" radiance errors (described in Section 3.3.3.2) which were often much larger than pure instrumental errors. For NIR-based retrievals, neglecting this geophysical noise in the MOPITT retrieval algorithm led to a high rate of nonconverged retrievals and prevented meaningful retrieval error estimation. This obstacle was overcome by (1) a new method implemented in the MOPITT Level 1 processor for quantifying radiance errors resulting from both instrumental noise and geophysical noise and (2) a new feature in the retrieval algorithm which increased the effective weight of the NIR measurements [Deeter et al., 2011].

The V5 release first introduced new MOPITT products based on (1) NIR observations and (2) simultaneous TIR and NIR observations [Deeter et al., 2013]. For V5 and subsequent versions, TIR-only, NIR-only and TIR-NIR retrievals are all produced operationally; each of these have relative strengths and weaknesses. The TIR-NIR product offers the greatest vertical resolution, and particularly the greatest sensitivity to CO in the lower troposphere. However, it also exhibits relatively large random retrieval errors and bias drift. Moreover, the main benefits of this product are only evident in daytime MOPITT observations over land. The TIR-only product offers the highest temporal stability and similar performance in variable observing situations (day and night, land and ocean). The NIR-only product is most suited for the analysis of CO total columns but is strictly limited to daytime observations over land.

For V5 and subsequent releases, TIR-only retrievals for the entire MOPITT record are based on the Difference radiances for Channels 5 and 7, and the Channel 5 Average radiance, whereas NIR-only retrievals are based on the ratio of the Channel 6 Difference and Average radiances. TIR-NIR products are based on the Difference radiances for Channels 5 and 7, the Channel 5 Average radiance and the ratio of the Channel 6 Difference and Average radiances. (Note that currently available MOPITT products do not exploit observations from Channels 1, 2, and 3 which were only operational from 2 March 2000 to 6 May 2001.)

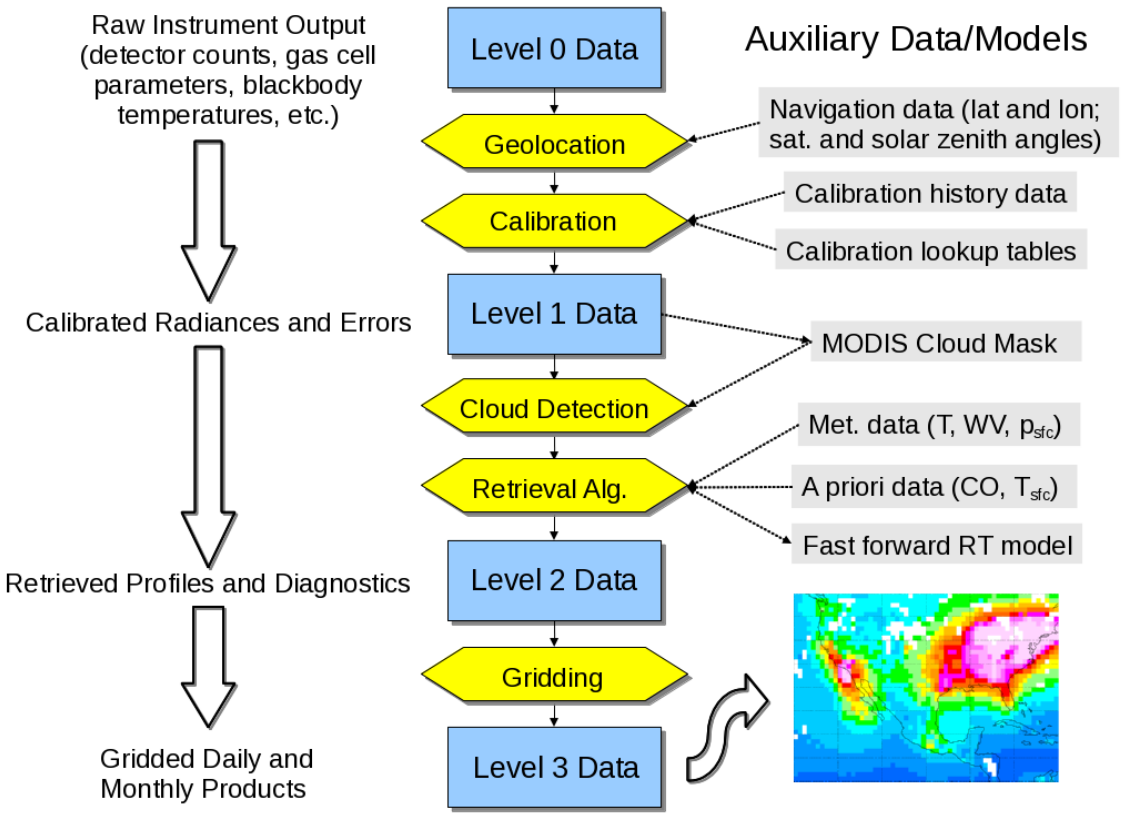

Figure 1: MOPITT data processing chain.

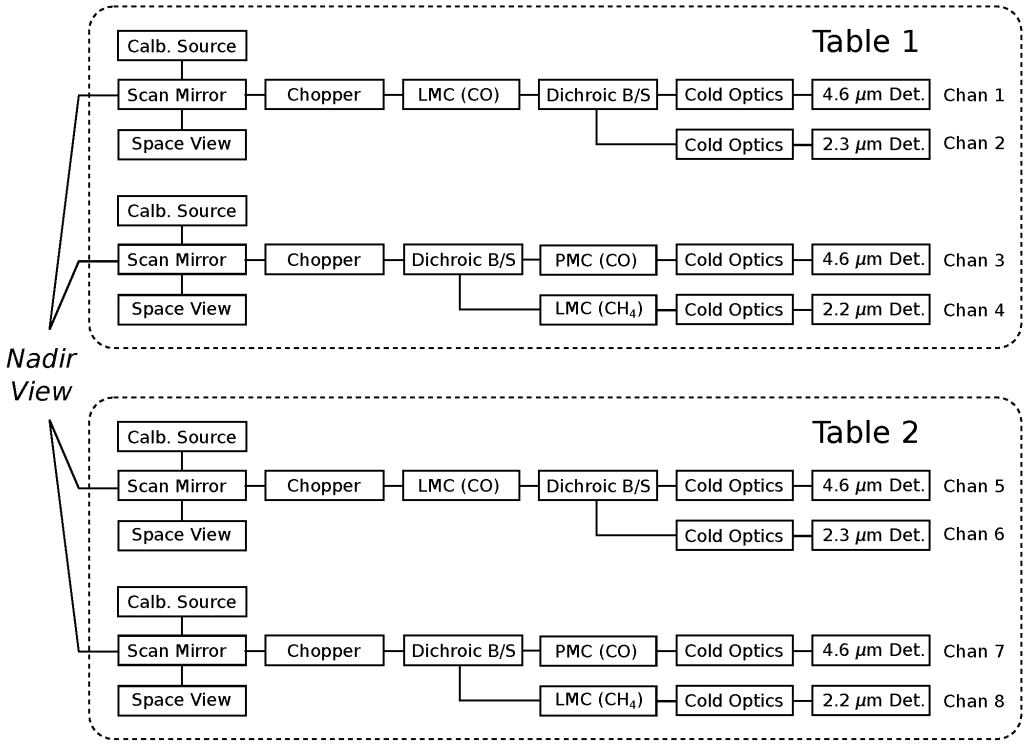

Figure 2: Detailed block diagram of the MOPITT instrument.

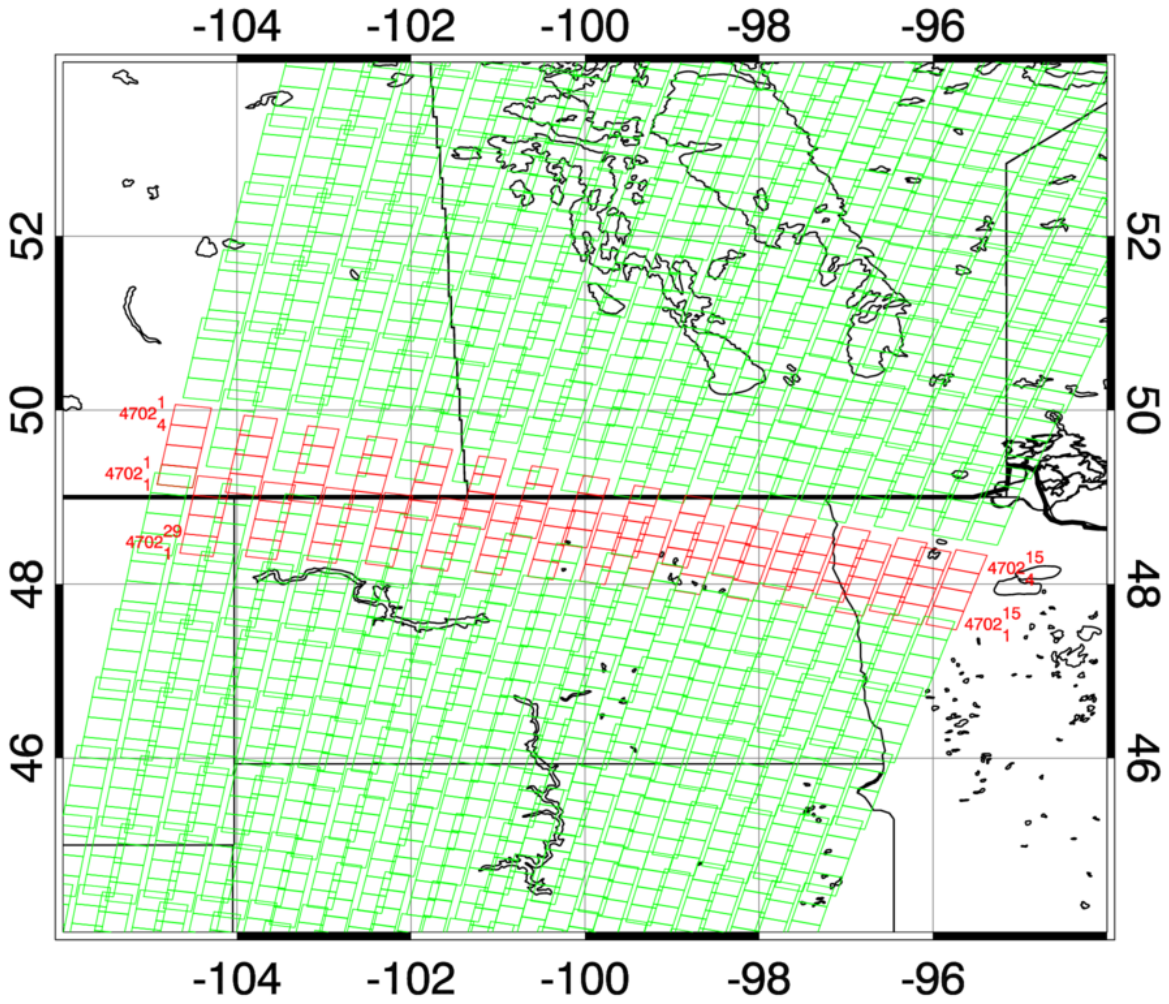

Figure 3: The footprints of MOPITT observations acquired 12 April 2010 near the border between Manitoba (Canada) and North Dakota (USA). Shown are several tracks acquired during a daytime, descending orbit. A single track (number 4702) is highlighted in red; some of the individual pixels in this track have been labeled as follows: $track^{stare}_{pixel}$. The size of a MOPITT pixel at nadir is $\sim$22x22 km^2.

Table 1: Nominal MOPITT Channel Characteristics.

Channel Characteristics	1	2	3	4	5	6	7	8
Gas Species	CO	CO	CO	CH_4	CO	CO	CO	CH_4
Nominal Gas Pressure (kPa)	20	20	7.5	80	80	80	3.8	80
Mid-Wavenumber (cm^{-1})	2166	4285	2166	4430	2166	4285	2166	4430
Wavenumber Range (cm^{-1})	52	40	52	139	52	40	52	139
Mid-Wavelength (μm)	4.617	2.334	4.617	2.258	4.617	2.334	4.617	2.258
Wavelength Range (μm)	0.111	0.022	0.111	0.071	0.111	0.022	0.111	0.071
Modulator Type & Number	LMC1	LMC1	PMC1	LMC2	LMC3	LMC3	PMC2	LMC4
Nominal Modulator Freq (Hz)	11.78	11.78	51.85	11.78	11.54	11.54	42.85	11.54
Nominal Chopper Freq (Hz)	518.5	518.5	518.5	518.5	600	600	600	600
Scan Mirror/Chopper Number	#1	#1	#2	#2	#3	#3	#4	#4
Calibration Source Number	#1	#1	#2	#2	#3	#3	#4	#4
Optical Table	#1	#1	#1	#1	#2	#2	#2	#2

Table 2: MODIS Cloud Diagnostics

Diagnostic	Content	Notes
1	number of "determined" MODIS pixels	i.e., tests were successful
2	percentage of cloudy MODIS pixels	-
3	percentage of clear MODIS pixels	-
4	average of "sun glint" MODIS flag	0=yes, 1=no
5	average of "snow/ice background" MODIS flag	0=yes, 1=no
6	average of "non-cloud obstruction" MODIS flag	0=yes, 1=no
7	average of "IR threshold test" MODIS flag	0=yes, 1=no
8	average of "IR temperature difference tests" MODIS flag	0=yes, 1=no
9	average of "visible reflectance test" MODIS flag	0=yes, 1=no
10	fraction of "determined" MODIS pixels	-

Table 3: MOPITT Cloud Descriptor Values

Descriptor value	MOPITT assignment	MODIS assignment	Notes
1	clear	-	MODIS data not available
2	clear	clear	-
3	cloudy	clear	-
4	clear	cloudy, low clouds	-
5	clear/cloudy	clear	used poleward of $\pm 65^{o}$ only
6	clear	cloudy, no low clouds	introduced in MOPITT V7, ocean observations only

Table 4: MOPITT Product Versions.

Product	Variants	Operational Period	CO State Vector	CO A Priori	Met. Fields	Retrieval Levels
V3	TIR	2002-2009	VMR	Fixed	NCEP	7
V4	TIR	2009-2012	log(VMR)	MOZART	NCEP	10
V5	TIR,NIR,TIR-NIR	2011-2016	log(VMR)	MOZART	NCEP	10
V6	TIR,NIR,TIR-NIR	2013-pres.	log(VMR)	CAM-chem	MERRA	10
V7	TIR,NIR,TIR-NIR	2016-pres.	log(VMR)	CAM-chem	MERRA-2	10

Table 5: Radiance bias correction factors applied to calculated MOPFAS radiances to compensate for observed radiance biases.

Product	Variant	Obs. Period	5A	7A	1D	3D	5D	7D	6A	6D
V3	TIR	Phase I	n/a	1.000	0.976	0.940	n/a	0.940	n/a	n/a
V3	TIR	Phase II	0.997	n/a	n/a	n/a	0.9855	0.920	n/a	n/a
V4	TIR	Phase I	n/a	1.000	0.976	0.940	n/a	0.940	n/a	n/a
V4	TIR	Phase II	0.997	n/a	n/a	n/a	0.9855	0.920	n/a	n/a
V5	TIR	all	0.9968	n/a	n/a	n/a	0.9857	0.970	n/a	n/a
V5	NIR	all	n/a	n/a	n/a	n/a	n/a	n/a	1.000	1.000
V5	TIR-NIR	all	0.9968	n/a	n/a	n/a	0.9857	0.970	1.000	1.000
V6	TIR	all	0.99685	n/a	n/a	n/a	0.98565	0.900	n/a	n/a
V6	NIR	all	n/a	n/a	n/a	n/a	n/a	n/a	1.000	1.000
V6	TIR-NIR	all	0.99685	n/a	n/a	n/a	0.98565	0.900	1.000	1.000
V7	TIR	all	0.997193	n/a	n/a	n/a	0.984704	0.920833	n/a	n/a
V7	NIR	all	n/a	n/a	n/a	n/a	n/a	n/a	1.000	0.99648
V7	TIR-NIR	all	0.997193	n/a	n/a	n/a	0.984704	0.920833	1.000	0.99648

References

Abel, P. G., P. J. Ellis, J. T. Houghton, G. Peckham, C. D. Rodgers, S. D. Smith, and E. J. Williamson (1970), Remote Sounding of Atmospheric Temperature from Satellites. II. The Selective Chopper Radiometer for Nimbus D, *Proc. Roy. Soc. Lond. A, 320,* 35-55, doi:10.1098/rspa.1970.0196.

Ackerman, S., R. Frey, K. Strabala, Y. Liu, L. Gumley, B. Baum, and P. Menzel (2010), Discriminating clear-sky from cloud with MODIS - Algorithm Theoretical Basis Document, Products: MOD35, ATBD Reference Number: ATBD-MOD-06.

Ackerman, S. et al. (2015), MODIS atmosphere L2 cloud mask product. NASA MODIS Adaptive Processing System, Goddard Space Flight Center, USA, doi:10.5067/MODIS/MOD35_L2.006.

Berman, R., P. Duggan, M. P. Le Flohic, A. D. May, and J. R. Drummond (1993), Spectroscopic technique for measuring the temperature and pressure cycle of a pressure modulator radiometer, *Appl. Opt., 32*, 6280-6283, doi:10.1364/AO.32.006280.

Clough, S. A., F. X. Kneizys, R. Davies, R. Gamache, and R. Tipping (1980), Theoretical line shape for H_2O vapor; Application to the continuum, in *Atmospheric Water Vapor*, edited by A. Deepak et al., pp. 25-46, Academic Press, New York.

Deeter, M. N., et al. (2003), Operational carbon monoxide retrieval algorithm and selected results for the MOPITT instrument, *J. Geophys. Res., 108(D14)*, 4399, doi:10.1029/2002JD003186.

Deeter M. N., D. P. Edwards, and J. C. Gille (2007), Retrievals of carbon monoxide profiles from MOPITT observations using lognormal a priori statistics, *J. Geophys. Res., 112* doi:10.1029/2006JD007999.

Deeter M. N., D. P. Edwards, J. C. Gille, and J. R. Drummond (2009), CO retrievals based on MOPITT near-infrared observations, *J. Geophys. Res., 114*, doi:10.1029/2008JD010872.

Deeter, M. N., et al. (2010), The MOPITT version 4 CO product: Algorithm enhancements, validation, and long-term stability, *J. Geophys. Res., 115*, doi:10.1029/2009JD013005.

Deeter, M. N., H. M. Worden, J. C. Gille, D. P. Edwards, D. Mao, and J. R. Drummond (2011), MOPITT multispectral CO retrievals: Origins and effects of geophysical radiance errors, *J. Geophys. Res., 116*, doi:10.1029/2011JD015703.

Deeter, M. N., S. Martínez-Alonso, D. P. Edwards, L. K. Emmons, J. C. Gille, H. M. Worden, J. V. Pittman, B. C. Daube, and S. C. Wofsy (2013), Validation of MOPITT version 5 thermal-infrared, near-infrared, and multispectral carbon monoxide profile retrievals for 2000-2011, *J. Geophys. Res., 118*, doi:10.1002/jgrd.50272.

Deeter, M. N., D. P. Edwards, J. C. Gille, and H. M. Worden (2015), Information content of MOPITT CO profile retrievals: Temporal and geographical variability, *J. Geophys. Res. Atmos., 120*, 12723-12738, doi:10.1002/2015JD024024.

Drummond, J. R. (1989), Novel correlation radiometer: The length-modulated radiometer, *Appl. Opt.,28*, 2451-2452, doi:10.1364/AO.28.002451.

Drummond, J. R. (1992), Measurements of Pollution in the Troposphere (MOPITT), in *The use of EOS for studies of atmospheric physics*, edited by J. C. Gille and G. Visconti, 77-101.

Drummond, J. R., J. Zou, F. Nichitiu, J. Kar, R. Deschambaut, and J. Hackett (2010), A review of 9-year performance and operation of the MOPITT instrument, *Adv. Space Res., 45*, 760-774, doi:10.1016/j.asr.2009.11.019

Drummond, J.R., J. Hackett and D. Caldwell (2016), Measurements Of Pollution In The Troposphere (MOPITT), in *Optical Payloads for Space Missions*, Shen-En Qian, Ed., Wiley.

Eck, T. F., B. N. Holben, J. S. Reid, O. Dubovik, A. Smirnov, N. T. O'Neill, I. Slutsker, and S. Kinne (1999), Wavelength dependence of the optical depth of biomass burning, urban, and desert dust aerosols, *J. Geophys. Res., 104*, 31333-31349, doi:10.1029/1999JD900923.

Edwards, D. P. (1992), GENLN2: A general line-by-line atmospheric transmittance and radiance model, version 3.0 description and users guide, *NCAR Technical Note NCAR/TN-367-STR*, National Center for Atmospheric Research, Boulder, CO, doi:10.5065/D6W37T86.

Edwards, D. P., C. M. Halvorson, and J. C. Gille, (1999), Radiative transfer modeling for the EOS Terra satellite Measurements of Pollution in the Troposphere (MOPITT) instrument, *J. Geophys. Res., 104,* 16755-16775, doi:10.1029/1999JD900167.

Edwards, D. P., and G. L. Francis (2000), Improvements to the correlated-k radiative transfer method: Application to satellite infrared sounding, *J. Geophys. Res., 105*, 18135-18156, doi:10.1029/2000JD900131.

Edwards, D. P., A. F. Arellano, and M. N. Deeter (2009), A satellite observation system simulation experiment for carbon monoxide in the lowermost troposphere, *J. Geophys. Res., 114*, D14304, doi:10.1029/2008JD011375.

Edwards, D. P., and G. L. Francis (2017), GENLN3: A general line-by-line atmospheric transmittance and radiance model, version 1.0 description and users guide, NCAR Technical Note, National Center for Atmospheric Research, Boulder, CO, *in preparation.*

Emmons, L. K., et al. (2010), Description and evaluation of the Model for OZone and Related chemical Tracers, version 4 (MOZART-4), *Geoscientific Model Dev., 3,* 43-67, doi:10.5194/gmd-3-43-2010.

Engelen, R. J., and G. L. Stephens (1999), Characterization of water-vapour retrievals from TOVS/HIRS and SSM/T-2 measurements, *Q. J. R. Meteorol. Soc., 125*, 331-351.

Goody, R. (1968), Cross Correlating Spectrometer, *J. Opt. Soc. Amer., 58,*, 900-908, doi:10.1364/JOSA.58.000900

Goody, R. (1969), Time variations in atmospheric N2O in eastern Massachusetts, *Planet. Space Sci., 17*, 1319-1320.

Hall, B. D., G. S. Dutton, and J. W. Elkins (2007), The NOAA nitrous oxide standard scale for atmospheric observations, *J. Geophys. Res., 112*, D09305, doi:10.1029/2006JD007954.

Hansen, J. E., and J. B. Pollack (1970), Near-infrared light scattering by terrestrial clouds, *J. Atmos. Sci., 27*, pp. 265-281, doi:10.1175/1520-0469(1970)027<0265:NILSBT>2.0.CO;2.

Hansen, J. E., and L. D. Travis (1974), Light scattering in planetary atmospheres, *Space Sci. Rev., 16*, 4, 527-610, doi:10.1007/BF00168069.

Ho, S.-P., D. P. Edwards, J. C. Gille, J. Chen, D. Ziskin, G. L. Francis, M. N. Deeter, and J. R. Drummond ((2005), Estimates of 4.7 μm surface emissivity and their impact on the retrieval of tropospheric carbon monoxide by Measurements of Pollution in the Troposphere (MOPITT), *J. Geophys. Res., 110*, doi:10.1029/2005JD005946.

Irvine, W. M., and J. B. Pollack (1968), Infrared optical properties of water and ice spheres, *Icarus, 8*, 2, 324-360, doi:10.1016/0019-1035(68)90083-3.

Katzoff S. (Ed.) (1971), *Remote Measurement of Pollution, NASA SP-285*, 253 pp., NASA Scientific and Technical Publications, National Aeronautics and Space Administration, Washington D.C., .

King, M. D., L. F. Radke, and P. V. Hobbs (1990), Determination of the spectral absorption of solar radiation by marine stratocumulus clouds from airborne measurements within clouds, *J. Atmos. Sci. 47*, 894-907, doi:10.1175/1520-0469(1990)047<0894:DOTSAO>2.0.CO;2.

King, M. D., Y. J. Kaufman, W. P. Menzel, and D. Tanre (1992), Remote sensing of cloud, aerosol, and water vapor properties from the moderate resolution imaging spectrometer (MODIS), *IEEE Trans. Geosci. Rem. Sens., 30*, 2-27, doi:10.1109/36.124212.

Lamarque, J.-F., et al. (2012), CAM-chem: description and evaluation of interactive atmospheric chemistry in the Community Earth System Model, *Geosci. Model Dev., 5*, 369-411, doi:10.5194/gmd-5-369-2012.

Luft, K.F. (1943), Über eine neue Methode der registrierenden Gasanalyse mit Hilfe der Absorption ultraroter Strahlen ohne spektrale Zerlegung, *Z. Tech. Phys., 24*, 97-104.

Ludwig, C. B., M. Griggs, W. Malkmus, and E. R. Bartle (1974), Measurement of air pollutants from satellites, 1: Feasibility considerations, *Appl. Opt., 13*, 1494-1509, doi:10.1364/AO.13.001494.

Lyapustin, A. et al. (2014), Scientific impact of MODIS C5 calibration degradation and C6+ improvements, *Atmos. Meas. Tech., 7*, 4353-4365, doi:10.5194/amt-7-4353-2014.

May, R. D., D. J. McCleese, D. M. Rider, J. T. Schofield, and C. R. Webster (1988), Tunable diode laser spectral diagnostic studies of a pressure modulator radiometer, *Appl. Opt., 27*, 3591-3593, doi:10.1364/AO.27.003591.

McMillin, L. M., L. J. Crone, M. D. Goldberg, and T. J. Kleespies (1995a), Atmospheric transmittance of an absorbing gas. 4. OPTRAN: A computationally fast and accurate transmittance model for absorbing gases with fixed and variable mixing ratios at variable viewing angles, *Appl. Opt.*, 34, 6269-6274, doi:10.1364/AO.34.006269.

McMillin, L. M., L. J. Crone, and T. J. Kleespies (1995b), Atmospheric transmittance of an absorbing gas. 5. Improvements to the OPTRAN approach, *Appl. Opt., 34*, 8396-8399, doi:10.1364/AO.34.008396.

Mokhov, I. L., and M. E. Schlesinger (1994), Analysis of global cloudiness: 2. Comparison of ground-based and satellite-based cloud climatologies, *J. Geophys. Res. Atmos., 99*, D8, 2156-2202, doi:10.1029/94JD00943.

Nakajima, T. Y., and M. D. King (1990), Determination of the optical thickness and effective particle radius of clouds from reflected solar radiation measurements. Part I: Theory, *J. Atmos. Sci., 47*, 1878-1893, doi:10.1175/1520-0469(1990)047<1878:DOTOTA>2.0.CO;2.

Nakajima, T. Y., M. D. King, J. D. Spinhirne, and L. F. Radke (1991), Determination of the optical thickness and effective particle radius of clouds from reflected solar radiation measurements. Part II: Marine stratocumulus observations, *J. Atmos. Sci.*, 48, 728-750, doi:10.1175/1520-0469(1991)048<0728:DOTOTA>2.0.CO;2.

Pan, L., D. P. Edwards, J. C. Gille, M. W. Smith, and J. R. Drummond (1995), Satellite remote sensing of tropospheric CO and CH_4: forward model studies of the MOPITT instrument, *Appl. Opt., 34,* 6976-6988, doi:10.1364/AO.34.006976.

Pan, L., J. Gille, D. P. Edwards, P. L. Bailey, and C. D. Rodgers (1998), Retrieval of carbon monoxide for the MOPITT instrument, *J. Geophys. Res., 103,* 32277-32290, doi:10.1029/98JD01828.

Pfister, G., J. C. Gille, D. Ziskin, G. Francis, D. P. Edwards, M. N. Deeter, and E. Abbott (2005), Effects of a spectral surface reflectance on measurements of backscattered solar radiation: Application to the MOPITT methane retrieval, *J. Atmos. Ocean Tech., 22,* 566-574, doi:10.1175/JTECH1721.1.

Pfund, A. H. (1939), Atmospheric Contamination, *Sci., 90,* 326-327, doi:90.2336.326/science.90.2336.326.

Reichle Jr., H. G., H. A. Wallio, J. C. Casas, and E. P. Condon (1986a), Gas filter radiometer for carbon monoxide measurements during the 1979 summer monsoon experiment (MONEX), *J. Geophys. Res. Atm., 91,* 9841-9848, doi:10.1029/JD091iD09p09841.

Reichle Jr., H. G., V. S. Connors, J. A. Holland, W. D. Hypes, H. A. Wallio, J. C. Casas, B. B. Gormsen, M. S. Saylor, and W. D. Hesketh (1986b), Middle and upper tropospheric carbon monoxide mixing ratios as measured by a satellite-borne remote sensor during November 1981, *J. Geophys. Res., 91*, 10865-10887, doi:10.1029/JD091iD10p10865.

Reichle, Jr., H. G., V. S. Connors, J. A. Holland, R. T. Sherrill, H. A. Wallio, J. C. Casas, E. P. Condon, B. B. Gormsen, and W. Seiler (1990), The distribution of middle tropospheric carbon monoxide during early October 1984, *J. Geophys. Res., 95*, 9845-9856, doi:10.1029/JD095iD07p09845.

Rienecker, M., et al. (2011), MERRA: NASA's Modern-Era Retrospective analysis for Research and Applications, *J. Climate, 24*, 3624-3648, doi:10.1175/JCLI-D-11-00015.1.

Rodgers, C. D. (2000), *Inverse methods for atmospheric sounding: Theory and practice*, Series on Atmospheric, Oceanic and Planetary Physics, 2, 238 pp., World Scientific, Singapore.

Roscoe, H. K., and R. J. Wells (1989), The variation of pressure, temperature and transmission within a pressure modulator: measurements with a high-compression modulator, *J. Quant. Spectrosc. Radiat. Transfer, 41*, 259-285, doi:10.1016/0022-4073(89)90122-2.

Rossow, W. B., and R. A. Schiffer (1999), Advances in understanding clouds from ISCCP, *Bulletin of the American Meteorological Society, 80*, 11, pp. 2261-2287, doi:10.1175/1520-0477(1999)080<2261:AIUCFI>2.0.CO;2.

Rothman L.S. et al. (2013), The HITRAN2012 molecular spectroscopic database, *J. Quant. Spectrosc. Radiat. Transfer, 130*, 4-50, doi:10.1016/j.jqsrt.2013.07.002.

Smith, S. D., and C. R. Pidgeon (1964), Application of Multiple Beam Interferometric Methods to the Study of CO_2 Emission at 15 μm, *Mémoires de la Société Royale des Sciences de Liége, 9,* 336-349.

Sun, J., S. Madhavan, X. Xiong, and M. Wang (2015), Long-term drift induced by the electronic crosstalk in Terra MODIS band 29, *J. Geophys. Res. Atmos., 120*, 9944-9954, doi:10.1002/2015JD023602.

Sun, J., S. Madhavan, and M. Wang (2016), Investigation and mitigation of the crosstalk effect in Terra MODIS band 30, *Remote Sens., 8*, 249, doi:10.3390/rs8030249.

Taylor, F. W. (1983), Pressure modulator radiometry, in *Spectroscopic Techniques*, edited by G. A. Vanasse, pp. 137-197, Academic Press, New York.

Tolton, B. T., and J. R. Drummond (1997), Characterization of the length-modulated radiometer, *Applied Optics, 36,* 5409-5420, doi:10.1364/AO.36.005409.

Worden, H. M., D. P. Edwards, M. N. Deeter, D. Fu, S. S. Kulawik, J. R. Worden, and A. Arellano (2013), Averaging kernel prediction from atmospheric and surface state parameters based on multiple regression for nadir-viewing satellite measurements of carbon monoxide and ozone, *Atmos. Meas. Tech., 6*, 1633-1646, doi:10.5194/amt-6-1633-2013.

Worden, H. M., M. N. Deeter, D. P. Edwards, J. Gille, J. Drummond, L. K. Emmons, G. Francis, and S. Martínez-Alonso (2014), 13 years of MOPITT operations: lessons from MOPITT retrieval algorithm development, *Ann. Geophys., 56(0)*, doi:10.4401/ag-6330.

Wylie, D. P., W. P. Menzel, H. M. Woolf, and K. I. Strabala (1994), Four years of global cirrus cloud statistics Using HIRS, *J. Climate, 7*, 4-18, doi:10.1175/1520-0442(1994)007<1972:FYOGCC>2.0.CO;2.

Wylie, D. P. and W. P. Menzel (1999), Eight years of high cloud statistics using HIRS, *J. Climate, 12*, 1, 170-184, doi:10.1175/1520-0442-12.1.170.